THE
PHYSICAL REVIEW

A journal of experimental and theoretical physics established by E. L. Nichols in 1893

SECOND SERIES, VOL. 169, NO. 1 5 MAY 1968

Hyperfine Effects in Muonic Bi and Pb†‡

R. J. POWERS*§
The Enrico Fermi Institute for Nuclear Studies and Department of Physics, The University of Chicago, Chicago, Illinois
(Received 3 August 1967)

We have investigated the K and L transitions in the muonic spectra of Bi^{209} and of the separated isotopes Pb^{206}, Pb^{207}, and Pb^{208}, using a Ge(Li) spectrometer. Our isotope shifts in Pb, in excellent agreement with the optical data, are half those predicted by the $A^{1/3}$ law. The agreement between our shifts and the optical shifts strongly suggests the absence of nuclear polarization by the muon. We have studied the $M1$ and $E2$ hyperfine (hf) interactions in Bi^{209}. The $M1$ results, although not sensitive enough to distinguish models of nuclear magnetization distributions, rule out a point magnetic dipole. The $E2$ constants, when used in conjunction with the measured isotone shift between Bi^{209} and Pb^{208}, suggest a quadrupole distribution produced by an $h_{9/2}$ proton and a slightly ($\sim$1%) deformed Pb^{208} core. We have examined the effects of $E3$ mixing of Bi^{209} nuclear levels on the K and L intensity ratios and on the interpretation of the hf constants.

I. INTRODUCTION

WE have investigated the K and L transitions in the muonic spectra of Bi^{209}, and of separated isotopes Pb^{206}, Pb^{207}, and Pb^{208}, using a Ge(Li) spectrometer.[1]

We had three reasons for studying these particular transitions: (1) To measure the isotope shift (I.S.) in muonic lead. The I.S.'s are directly related to the change in charge distributions as a function of neutron number, and have been measured very precisely by optical spectroscopy.[2] Muonic x rays serve as a useful complement to these optical measurements, inasmuch as it is difficult to extract accurate absolute shifts from the latter because of theoretical uncertainties. Such uncertainties relate to the value of the electron wave functions at the nucleus, and to the magnitude of the shielding effects, and are typically problems of the order of 20%.[3]

On the other hand, relative isotope shifts can be determined quite accurately from optical spectra because for this case these uncertainties essentially cancel. Conversely, absolute muonic I.S.'s can be calculated quite easily, although the interpretation of the data may be obscured by nuclear polarization effects. If the change in transition energy due to polarization is large—and the literature provides us with estimates ranging from 1[4] to 50 keV[5]—then differences in polarization energy from one isotope to the other can contribute to the observed I.S. Similarly, the observed relative I.S.'s would also be in error with respect to the ratio of the true volume effects, i.e., the relative I.S.'s observed spectroscopically. Thus, by comparing the corresponding (sufficiently precise) muonic and electronic I.S., one can set limits on the polarization contribution. Once this is established to be small, the absolute muonic I.S. can be interpreted with confidence and used to put the spectroscopic measurements on a sound footing.

Lead was chosen for the comparison between muonic and optical I.S.'s because the optical data for this element are particularly accurate and amenable to theoretical interpretation. A brief summary of the pertinent theory is given in Sec. II A.

(2) To study the hyperfine structure (hfs) of muonic Bi^{209}. In particular, we wished to study the magnetic ($M1$) hfs, i.e., the interaction between the muon and the nuclear magnetization. Since the muon penetrates

† Research supported by the U. S. Office of Naval Research and National Science Foundation Grant No. GP 6135 (Research).
‡ A thesis submitted to the Department of Physics, The University of Chicago, in partial fulfillment of the requirements for the Ph.D. degree.
* National Science Foundation Predoctoral Fellow, 1961–66.
§ Present address: Virginia Associated Research Center, Newport News, Va. and Virginia Polytechnic Institute, Blacksburg, Va.
[1] For preliminary reports summarizing our findings see R. D. Ehrlich, D. Fryberger, D. A. Jensen, C. Nissim-Sabat, R. J. Powers, B. A. Sherwood, and V. L. Telegdi, Phys. Rev. Letters **16**, 425 (1966); Phys. Letters **23**, 468 (1966); V. L. Telegdi, in Proceedings of the Williamsburg Conference on Intermediate Energy Physics, 1966, p. 77 (unpublished).
[2] A. Steudel, Z. Physik, **133**, 438 (1952).
[3] P. Brix and H. Kopfermann, Rev. Mod. Phys. **30**, 517 (1958).
[4] W. Greiner, Z. Physik **164**, 374 (1961).
[5] L. N. Cooper and E. M. Henley, Phys. Rev. **92**, 801 (1953).

the nucleus to a much greater extent than an electron, muonic hfs is much more sensitive to the effects predicted by Bohr and Weisskopf,[6] who showed that the $M1$ hfs reflects not only the finite extent of the nuclear magnetization but also its detailed distribution. Theoretical estimates of these effects in muonic atoms have been given by LeBellac[7] and by Winston.[8] At the time we began these studies, $M1$ hfs effects had not been directly observed in muonic spectra. Subsequently, we learned that similar investigations were in progress at Columbia[9] and Carnegie Tech.[10] Of course, observations of $M1$ hfs effects had already been made in muon-capture experiments.[8,11,12]

Bi^{209} was chosen because its large $M1$ moment (=4.0802 nm)[13] and high Z lead to the largest effect among all accessible targets. It is, furthermore, monoisotopic and should exhibit, for obvious reasons, effects due to the finite distribution of nuclear magnetization particularly well. However, even in this case hfs splittings are at most 5 keV in the 6-MeV $2p_{1/2} \rightarrow 1s_{1/2}(K\alpha_2)$ transition, i.e., smaller than the resolution of the best Ge(Li) spectrometers. For this reason the quantitative study of these phenomena must necessarily be based on a change in line shape. This poses delicate experimental problems which we solved by observing corresponding transitions in Bi^{209} and Pb^{206}, an isotope which leads to no hfs, simultaneously.

We also continued our earlier studies of the electric quadrupole ($E2$) charge distribution.[14] In muonic Bi^{209}, the $E2$ interaction is about three times larger than the $M1$ interaction, and is hence readily observed. Our interest in this interaction lay also in the rather poor knowledge of the quadrupole moment of Bi^{209}, whose spectroscopic value[15–17] is buried in theoretical uncertainties. From our simultaneous measurements of the pairs (Bi^{209}, Pb^{206}) and (Pb^{206}, Pb^{208}), we obtained a value for the $K\alpha$ isotone shift (Bi^{209}, Pb^{208}), i.e., for the increase in muon binding energy produced by adding a proton to Pb^{208}. This isotone shift gives us additional information for interpreting the quadrupole distribution in Bi^{209}. A more complete discussion of the theory can be found in Sec. II B.

(3) To measure the intensity ratios of the K and L fine-structure (fs) components in muonic Bi^{209} and the lead isotopes. Anomalies in these ratios for Bi^{209} had been observed by various groups.[18,19] A purely nuclear mechanism for explaining these anomalies was suggested by Hüfner,[20] who subsequently[21] also discussed alternate or at least complementary atomic mechanisms. Since such a nuclear mechanism could affect the interpretation of the hyperfine splittings, it was of interest to verify such a process by looking for the γ rays from the de-excitation of the admixed nuclear states. The consequences of these nuclear mechanisms are discussed in Sec. II C.

Furthermore, it was of interest to search for similar anomalies in the neighboring Pb isotopes. If the anomalies were exhibited by some but not all of these isotopes, then the effect would probably be of a nuclear rather than atomic origin.

II. SUMMARY OF THEORY OF hf EFFECTS IN MUONIC Pb AND Bi

A. Isotope Shift in Ordinary Atoms

In heavy elements one observes a volume effect, so called because the nucleus can no longer be treated as a point. This effect—which is the only one relevant to the elements under examination—is thoroughly discussed by Kopfermann.[22]

We summarize here the more important results concerning the isotope shift of an s level using Kopfermann's notation. The change δE in the energy of an electron due to a change δR_u in the nuclear radius R_u (such as produced by the addition of a neutron) can be factored as

$$\delta E = C(Z, R_u, \delta R_u/R_u) F(Z_a, Z_i, \sigma), \qquad (1)$$

where F is proportional to the probability density of the electron at the nucleus and depends on electronic parameters only. Specifically, Z_a and Z_i are the effective "outer" and "inner" nuclear charges seen by the electron and σ is the principal quantum defect. Conversely, the function C depends only on the nuclear parameters indicated as its argument.

A second source of isotope shift, important in light elements only, is known as the reduced mass shift and is due to the fact that the nucleus is not infinitely heavy, relative to the electron. Hence the effective mass of the electron is reduced by the motion of the nucleus about the center of gravity. For the pair of isotopes (Pb^{206}, Pb^{208}) this effect is 0.03 keV for the K muonic transitions, beyond the accuracy of this experiment.

[6] A. Bohr and V. F. Weisskopf, Phys. Rev. **77**, 94 (1950).
[7] M. Le Bellac, Nucl. Phys. **40**, 645 (1963).
[8] R. Winston, Phys. Rev. **129**, 2766 (1963).
[9] T. T. Bardin, R. Barrett, R. C. Cohen, S. Devons, D. Hitlin, E. Macagno, C. Nissim-Sabat, J. Rainwater, K. Runge, and C. S. Wu, Phys. Rev. Letters **16**, 429 (1966).
[10] S. Raboy, R. E. Coté, R. Guso, R. A. Carrigan, Jr., A. Gaigalas, R. B. Sutton, and C. C. Trail, Bull. Am. Phys. Soc. **11**, 129 (1966).
[11] G. Culligan, J. F. Lathrop, V. L. Telegdi, R. Winston, and R. A. Lundy, Phys. Rev. Letters **7**, 458 (1961).
[12] R. A. Lundy, W. A. Cramer, G. Culligan, V. L. Telegdi, and R. Winston, Nuovo Cimento **24**, 549 (1961).
[13] K. Siegbahn, *Alpha, Beta, and Gamma-Ray Spectroscopy* (North-Holland Publishing Co., Amsterdam, 1965), p. 1636.
[14] S. Raboy, C. C. Trail, J. A. Bjorkland, R. D. Ehrlich, R. J. Powers, and V. L. Telegdi, Nucl. Phys. **73**, 353 (1965).
[15] H. Schüler and T. Schmidt, Z. Physik **99**, 717 (1936).
[16] R. S. Title and K. H. Smith, Phil. Mag. **5**, 1281 (1960).
[17] V. S. Korol'kov and A. G. Makhanek, Opt. i Spektroskopiya **12**, 163 (1962) [English transl.: Opt. Spectry. **12**, 87 (1962)].
[18] W. Frati and J. Rainwater, Phys. Rev. **128**, 2360 (1962).
[19] H. L. Acker, G. Backenstoss, C. Daum, J. C. Sens, and S. A. DeWit, Phys. Letters **14**, 317 (1965).
[20] J. Hüfner, Z. Physik **190**, 81 (1966).
[21] J. Hüfner, in Proceedings of the Williamsburg Conference on Intermediate Energy Physics, 1966, p. 87 (unpublished).
[22] H. Kopfermann, *Nuclear Moments* (Academic Press Inc., New York, 1958), pp. 167–175.

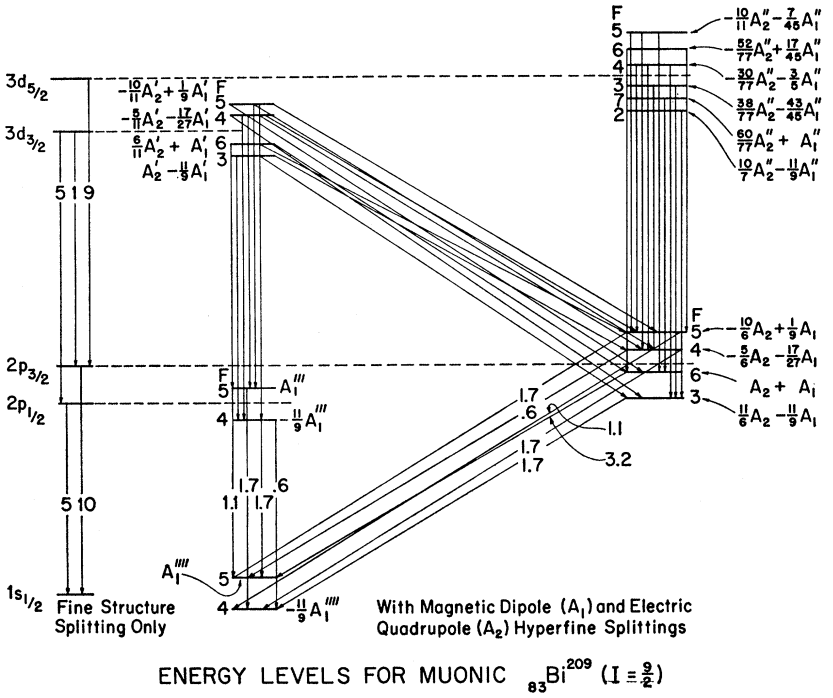

FIG. 1. Energy levels for muonic Bi^{209}. This drawing is not to scale. The left side of the figure shows levels unperturbed by hfs. The remainder of the figure shows the splitting due to magnetic dipole (A_1) and electric quadrupole (A_2) splittings. Allowed transitions are indicated by arrows. The superimposed numbers on the arrows indicate the relative intensities. The numeral next to each hyperfine level indicates the total angular momentum.

Of course a shift of an energy level is never measured directly. Only the shifts of transitions are measured, and these represent shifts in the initial and final states. However, electrons in orbits with $l>0$ penetrate the nucleus only slightly, and hence their shifts can generally be neglected.

Unfortunately, there are difficulties in interpreting the experimental results in ordinary atoms. Usually, the isotope shift (referred to the ionization limit) is attributed to the valence electrons alone, i.e., the closed shells of the atom are treated as unaffected by the penetration of the valence electron. However, when a valence electron is removed by ionization, so are its shielding effects. The resulting change is at best calculable and cannot be experimentally detected. Therefore, all empirical values of C are written as βC_{expt}, where $\beta(\approx 1)$ is an empirical factor allowing for this effect. An uncertainty is introduced in the factor F by the charge density at the nucleus for a generally multielectron atom. These uncertainties in the interpretations of the optical data are discussed by Breit[23] and by Kopfermann,[22] and estimates of uncertainties in C_{expt} as large as 20% are made.

We undertook the study of the muonic Pb isotope shifts because (1) the corresponding optical data are among the most accurately known experimentally; (2) these optical data are readily interpreted because a $(6p^2\,{}^3P_2\text{-}6p7s\,{}^3P_1)$ transition is involved; (3) Pb^{208} is a doubly magic nucleus.

[23] G. Breit, Rev. Mod. Phys. **30**, 507 (1958).

B. Atomic Hyperfine Interactions

In this section we present a brief summary of the fundamental notions underlying atomic hfs, with particular emphasis on those aspects that are relevant to muonic Bi^{209}. The $n\leq 3$ levels of this system are shown in Fig. 1, omitting the $2s$, $3s$, and $3p$ states as these are only weakly populated in the atomic cascade.[24] For the K lines ($2p \rightarrow 1s$) the intensities of the transitions connecting these levels, computed with certain assumptions, are also indicated.

Levels with $l>0$ are split by spin-orbit coupling into fs doublets with $j=l\pm\frac{1}{2}$; these splittings can be computed exactly if the monopole potential $V(r)$, produced by the nuclear charge distribution $\rho_N(\mathbf{R})$, is given.

For a nucleus of spin $I\neq 0$, the levels of given j will in general be further split (into states characterized by a total angular momentum $\mathbf{F}=\mathbf{I}+\mathbf{j}$) by interactions between the muon charge cloud and multipole moments of ρ_N and/or by the magnetic interaction between the muon current $\mathbf{j}_\mu(\mathbf{r})$ and moments of the nuclear current distribution $\mathbf{J}_N(\mathbf{R})$. The importance of these hf interactions decreases as the order of the moments increases, and it is, even for muons, sufficient to retain only the lowest terms, viz., the electric quadrupole ($E2$) and the magnetic dipole ($M1$) hf couplings.

Contrary to the situation in ordinary atoms, the muonic $E2$ hf interaction is larger than the $M1$, and was indeed the first to be discussed.[25] Its expectation

[24] Y. Eisenberg and D. Kessler, Nuovo Cimento **19**, 1195 (1961).
[25] J. Wheeler, Phys. Rev. **92**, 812 (1953).

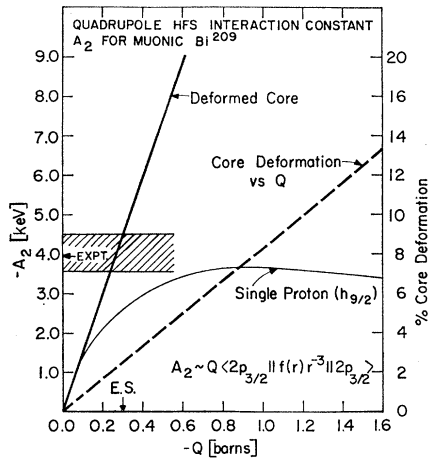

FIG. 2. Plot of A_2 as a function of the quadrupole moment Q of Bi^{209} for two opposite assumptions: (a) that Q is entirely due to the lone proton, (b) that it is entirely due to a deformed Pb^{208} core. The hatched strip indicates the experimental values of A_2 (Refs. 1 and 9). The right-hand scale gives the percentage core deformation versus Q for case (b).

value for a state F can be factored as

$$W(E2)_F = A_2\langle P_2(\mathbf{I},\mathbf{j})\rangle_F, \tag{2}$$

where the purely geometrical quantity $P_2(\mathbf{I},\mathbf{j})$ is the quantum-mechanical analog of $P_2(\theta)$ with $\cos\theta = \mathbf{I}\cdot\mathbf{j}/Ij$. It is given by[26]

$$\langle P_2(I,j)\rangle = \frac{\frac{3}{2}C(C+1)-2I(I+1)j(j+1)}{I(2I-1)j(2j-1)}, \tag{3}$$

where $C=F(F+1)-I(I+1)-j(j+1)$. The hf constant A_2 depends on the dynamics and can be written in the appealingly symmetric form

$$A_2 = -e^2\langle IIjj|\frac{R^2P_2(\hat{R})r^2P_2(\hat{r})}{r_>{}^5}|IIjj\rangle, \tag{4}$$

where the state is labeled as $|\mathrm{Im}_I jm_j\rangle$, and $r_>$ is the larger of the coordinates r and R. Conventionally, the quadrupole moment of a nucleus is defined as

$$Q = 2\langle II|R^2P_2(\hat{R})|II\rangle, \tag{5}$$

and (4) becomes in the limit of a point nucleus ($r_> \to r$)

$$A_2{}^{\mathrm{pt}} = -\tfrac{1}{2}e^2Q\langle jj|r^{-3}P_2(\hat{r})|jj\rangle = \tfrac{1}{4}e^2Q\langle r^{-3}\rangle_{n,j}(2j-1)/(2j+2), \tag{6}$$

a well-known result.[27] Formally, one can introduce a form factor $f(r)$ and write (4) as

$$A_2 = \tfrac{1}{4}e^2Q\langle f(r)r^{-3}\rangle_{n,j}(2j-1)/(2j+1). \tag{7}$$

The $f(r)$ depends on the nuclear model, and has been estimated for various hypotheses about $\rho_N(\mathbf{R})$[14,25,28]; once $f(r)$ is chosen, one can define a quantity f_q through

$$\langle f(r)r^{-3}\rangle_{n,j} \equiv f_q\langle r^{-3}\rangle_{n,j}, \tag{8}$$

i.e.,

$$A_2 = f_qA_2{}^{\mathrm{pt}},$$

so that f_q is the reduction of the hfs interaction from its point-quadrupole value (6). It is important to note that one always measured at best the product f_qQ, so that it is difficult to learn about the details of $f(r)$ without independent knowledge of the scale factor Q (see, however, Sec. V B).

For orientation purposes, it is useful to estimate f_q following Wheeler,[25] who assumed (a) that Q is due to a δ-like (surface-charge) distribution, and (b) that hydrogenic Schrödinger wave functions can be used in (8).

For $n=2, l=1$, he gives

$$f_q(x) \cong 1/(1+0.1x^2)^2, \tag{9}$$

where $x \equiv R_u(Z/a_0) =$ nuclear radius/Bohr radius.

Similarly, for $n=3, l=2$, one finds

$$f_q'(x) = 1/(1+0.004x^2)^2. \tag{10}$$

We can now estimate the $E2$ constants for Bi^{209}, for which nucleus $Q=-0.4$ b,[15] $R_u=7.1$ F, $x=2.3$, $f_q=0.43$ and $f_q'=0.96$.

$$\begin{aligned} &A_2(2p_{3/2}) = A_2 \approx f_q(2/4\times5\times24)W_0 = -3.57 \text{ keV},\\ &A_2(3d_{3/2}) = A_2' \approx f_q'(2/4\times5\times405)W_0 = -0.46 \text{ keV},\\ &A_2(3d_{5/2}) = A_2'' \approx f_q'(4/4\times7\times405)W_0 = -0.65 \text{ keV}, \end{aligned} \tag{11}$$

where we have used the convenient unit

$$W_0 = Z^3(Q/a_0{}^2)(e^2/a_0) = -1.99 \text{ MeV}.$$

Note that the finite-quadrupole correction is small for the $3d$ states ($f_q \approx 1$).

For Bi^{209}, a single-particle (about a Pb^{208} central core) description is particularly attractive. Using (4), we can readily write A_2 for this model:

$$A_2 = \frac{e^2}{4}\frac{2j-1}{2j+2}\sum_{i=1}^{A}\langle II|\epsilon_iP_2(\hat{R}_i)[R_i{}^2\langle j|r^{-3}|j\rangle_> + R_i{}^{-3}\langle j|r^2|j\rangle_<]|II\rangle, \tag{12}$$

where $|II\rangle = \psi_I{}^I(\mathbf{R}_1,\cdots,\mathbf{R}_i,\cdots,\mathbf{R}_A)$ is the product wave function, ϵ_i is the effective charge on the ith nucleon, and $|j\rangle$ is the Dirac radial function, i.e., $\langle j|j\rangle = f^2+g^2$. The subscript $<$ ($>$) defines the range of integration, i.e., $r<R_i$ ($>R_i$). If a single orbital $|II\rangle$ is retained in the sum (12), then both Q and $f(r\alpha)$ (hence f_q) are uniquely given in terms of the length parameter α of that orbital; we shall return to this point in Sec. V B.

[26] H. Casimir, *On the Interaction Between Atomic Nuclei and Electrons* (W. H. Freeman and Co., San Francisco, 1963).

[27] Our definition of $A_2{}^{\mathrm{pt}}$ corresponds to Kopfermann's quantity $\frac{1}{4}b$ (Ref. 22, p. 154).

[28] S. A. DeWit, G. Backenstoss, C. Daum, and J. C. Sens, Nucl. Phys. 87, 657 (1966).

Equation (12) has been evaluated by Le Bellac,[7] who quotes for Bi^{209} (with $\alpha^{-1}=0.33$ F and $Q=-0.44$ b).

$$A_2(2p_{3/2})=-3.02 \text{ keV}. \tag{13}$$

This value for α was obtained by[29] equating the mean-square radius for all nucleons in Bi^{209} to the equivalent radius obtained by

$$R_u=1.2\times A^{1/3} \text{ F}. \tag{14}$$

A more common procedure is to equate the mean-square radius for all protons in Bi^{209} (since it is the charge radius and not the nuclear radius measured by muonic x rays or electron scattering) to $\frac{3}{5}$ of the equivalent radius. This procedure gives a value of $\alpha^{-1}=0.4$ F and $Q=-0.3$ b.

In Fig. 2 we give a plot of the single-particle prediction for A_2 as a function of Q which is related to the parameter α through

$$Q_{\rm sp}=-52/11\alpha^2. \tag{15}$$

A_2 was calculated using harmonic-oscillator wave functions for the $h_{9/2}$ proton, and relativistic muon wave functions for a charge distribution ρ_N of the Fermi type, with the electron-scattering values[30] for the half-density radius $c=6.59$ F and skin thickness $s=2.5$ F.

A_2 decreases with increasing Q after going through a maximum because as the radius of the single proton orbit is increased, the muon finds itself more and more "inside the quadrupole moment," where its $E2$ interaction is greatly reduced. The single-particle model yields at most $A_2=-3.8$ keV. But this would imply $Q\approx-1$ b, i.e., almost three times the spectroscopically observed value of ~-0.4 b. On the other hand, if we adopt this observed Q, as determined by atomic-beam[16] or optical methods,[15] we predict $A_2\simeq-2.8$ keV.

We can also compute A_2 assuming that the quadrupole moment of Bi^{209} is in part or altogether due to a slightly deformed Pb^{208} core. The heavy straight line marked "Core Deformation," to be used with the right-hand scale, gives the percentage deformation [defined as $\frac{4}{3}(\frac{1}{5}\pi)^{1/2}(\Delta R/R_0)\times100$] required to produce a given Q.

We shall resume our discussion of a model for the quadrupole moment of Bi^{209} in Sec. V B.

We now turn to the $M1$ hf interaction; here the energy can again be factored in the form

$$W(M1)_F=A_1\langle P_1(\mathbf{I},\mathbf{j})\rangle_F, \tag{16}$$

where $\langle P_1\rangle_F$ is the usual Landé factor. The hf constant can be written in the symmetric form

$$A_1=-\tfrac{1}{2}\langle II\,j(l)j\,|\,(\mathbf{R}\times\mathbf{J}_N)_z(\mathbf{r}\times\mathbf{j}_\mu)_z\,|\,II\,j(l)j\rangle/r_>^3, \tag{17}$$

where $\mathbf{R},\mathbf{J}_N$ are the nuclear coordinate and current operators, and the other symbols have the same meaning as in Eq. (4), except that the orbital momentum l of the lepton is exhibited. In Eq. (17), one attributes all magnetization to currents, setting the problem of intrinsic (spin) magnetization temporarily aside. In the point-dipole limit ($r_>\to r$), Eq. (17) becomes

$$A_1^{\rm pt}=-\langle II\,|\,\tfrac{1}{2}(\mathbf{R}\times\mathbf{J}_N)_z\,|\,II\rangle \times\langle j(l)j\,|\,r^{-3}(\mathbf{r}\times\mathbf{j}_\mu)_z\,|\,j(l)j\rangle, \tag{18}$$

where the first factor by definition is the nuclear moment

$$\mu_I=g_I\mu_N I,$$

while the second is identified as an average magnetic field at $r=0$, i.e.,

$$A_1^{\rm pt}=-g_I\mu_N I\langle j(l)j\,|\,H_z(0)\,|\,j(l)j\rangle. \tag{19}$$

It is traditional to evaluate Eq. (18) using the Dirac formalism; this yields

$$\langle j(\kappa)j\,|\,H_z(0)\,|\,j(\kappa)j\rangle = -\frac{2e\kappa}{j+1}\int_0^\infty fgr^{-2}dr=\tfrac{2}{3}\mu_0\langle\delta(r)\rangle, \qquad (l=0) \tag{20a}$$

$$\langle j(\kappa)j\,|\,H_z(0)\,|\,j(\kappa)j\rangle=2\mu_0\frac{l(l+1)}{j(j+1)}\langle r^{-3}\rangle, \qquad (l\neq0) \tag{20b}$$

$$[\kappa=\mp(j\pm\tfrac{1}{2}) \quad \text{for} \quad j=l\pm\tfrac{1}{2}],$$

where we have indicated the nonrelativistic limits, in particular the Fermi contact term (20a). One can,[31] however, obtain these limits directly by computing the field as the expectation value of the expression

$$H_z=(8\pi/3)\mu_0 g_S S_z\delta(\mathbf{r})+(\mu_0/r^3)(g_s\hat{a}_z+g_l L_z), \tag{21}$$

where $a_z=-\frac{1}{2}[\mathbf{S}-3(\mathbf{S}\cdot\mathbf{r})\hat{r}]_z$, $g_s=-2$, and $g_l=-1$; note that the r^{-3} part of Eq. (21) is to be used only for $r\neq0$. We reproduce Eq. (21) here in this form because an analogous expression arises from the nuclear part of Eq. (18) in a certain model.

The simplest model for the nuclear magnetization that enables one to evaluate Eq. (17) consists in assuming that this quantity is contributed by a moment distributed isotropically inside the nucleus; this is analogous to the magnetization of an atomic s state (but for spin I not necessarily $=\frac{1}{2}$) with this assumption

$$\tfrac{1}{2}\langle II\,|\,\mathbf{J}_N\times\mathbf{R}\,|\,II\rangle\equiv\mu_N g_I I\int_0^\infty d^3R\,[\Psi_I{}^I(R)]^2 \equiv\mu_N g_I\int_0^\infty d^3R\,\rho_M(R), \tag{22}$$

where ρ_M is spherically symmetric. For simplicity, we assume the lepton in an s state $\Psi(r)$, and thus can use

[29] M. Le Bellac (private communication).
[30] G. J. C. Van Niftrik and R. Engfer, Phys. Letters **22**, 490 (1966).
[31] H. A. Bethe and E. E. Salpeter, *Quantum Mechanics of One- and Two-Electron Atoms* (Springer-Verlag, Berlin, 1957), Sec. 22.

TABLE I. Calculated values of A_1 and A_2 (keV).

	Our calculations[a]		Le Bellac[b]	
	Finite[b] $Q_{sp}=-0.3$ b	Point moment[b]	Finite $Q_{sp}=-0.44$ b	Point moment
$A_1(1s_{1/2})$	2.00	3.14	1.63	3.02
$A_1(2p_{1/2})$	1.07	1.73	0.84	1.62
$A_1(2p_{3/2})$	0.50	0.80	0.83	...
$A_1(3d_{3/2})$	0.3	0.3	...	...
$A_1(3d_{5/2})$	0.1	0.1	...	...
$A_2(2p_{3/2})$	−2.8	−4.5[c]	−3.02	−6.55[c]
$A_2(3d_{3/2})$	−0.6	−0.6	...	...
$A_2(3d_{5/2})$	−0.7	−0.7	...	...

[a] These values are obtained for wave functions with configuration mixing. For pure $h_{9/2}$ wave function, they are reduced by 17%.
[b] Reference 7.
[c] Assumed $Q=Q_{sp}$.

the first term in Eq. (21) for either current in Eq. (17);

$$A_1(1s_{1/2})=(8\pi/3)(\mu_N g_I I)\mu_0\int_0^\infty d^3r\,\rho_M(r)\Psi_{1s_{1/2}}{}^2(r). \quad (23)$$

As a further simplification, it is convenient to assume that the magnetization and charge of the nucleus are distributed in the same way, i.e., that $\rho_M(R)=\rho_N(R)$. One may then use the quantity

$$\int_0^\infty d^3r\,\rho_N(r)\Psi_{1s_{1/2}}{}^2(r)\equiv Z_{\rm eff}{}^4/\pi a_0{}^3 Z, \quad (24)$$

which has been tabulated in the literature[32] (because it is useful for computing muon capture rates). Using this quantity, one can write[8]

$$A_1(1s_{1/2})=(8\pi/3)(\mu_N g_I I)\mu_0 Z_{\rm eff}{}^4/Z\pi a_0{}^3$$
$$=A_1{}^{\rm pt}(1s_{1/2})(Z_{\rm eff}{}^4/Z^4)=1.52\ \text{keV}. \quad (25)$$

Describing the nucleus nonrelativistically[33] in terms of the shell model, one can write down the quantum-mechanical analog of Eq. (17):

$$A_1=\frac{-2\mu_N e\kappa}{j+1}\int d^3R\sum_{i=1}^{A}\Psi_I{}^{M=I}(R_i)$$
$$\times\begin{bmatrix} g_l L_z\left[\int_{R_i}^\infty\frac{fg}{r^2}dr+\int_0^{R_i}\frac{r}{R_i{}^3}fgdr\right] \\ g_s\left[S_z\int_{R_i}^\infty\frac{fg}{r^2}dr+a_z\int_0^{R_i}\frac{r}{R_i{}^3}fgdr\right]\end{bmatrix}\Psi_I{}^{M=I}(R_i). \quad (26)$$

This form is made plausible by Eqs. (17) and (21) and was proved in Refs. 6 and 7. The decomposition of the nuclear magnetization into spin and orbital part is the essence of the Bohr-Weisskopf[6] effect. Le Bellac[7] has evaluated Eq. (26) for muonic Bi, using (a) numerical relativistic muon wave functions as given by Ford and Wills[34] fitted to a fourth-order polynomial, (b) harmonic oscillator shell-model wave functions with $\alpha=0.33$ F^{-1} ($Q_{sp}=-0.44$ b). We have performed the same calculations (a) using more exact muon wave functions, and (b) $\alpha=0.40$ F^{-1} ($Q_{sp}=-0.30$ b), a value which is more consistent with electron scattering data (see Sec. V B).

In Table I we give a comparison of our values of A_1 and A_2 calculated for point and distributed moments with those of Le Bellac. The only serious discrepancy is in the value of $A_1(2p_{3/2})$. Our A_1 values have been increased by $\sim 20\%$ to include the effects of configuration mixing computed by Le Bellac.

The intensities indicated in Fig. 1 were taken from the computations done by White and Eliason[35] for ordinary atoms. They depend essentially only on the angular-momentum quantum numbers, inasmuch as the following assumptions are made:

(1) All levels decay only by radiative $E1$ transitions;
(2) the splitting of the fs doublets and the difference in the radial wave functions of their members ($j=l\pm\frac{1}{2}$) is neglected;
(3) the $4f$ levels are initially populated according to their statistical weights $(2j+1)$.

These assumptions are not equally justified for high-Z muonic atoms. Aside from the $E1$ radiative transitions, the levels may be depopulated by nonradiative atomic processes (e.g., Auger effects) and by a variety of nuclear processes. The former are negligible,[21] while the latter may be quite important in certain cases. Among these is Bi^{209}, where considerable mixing of muonic and nuclear levels arises from $E3$ coupling, a situation which shall be discussed in Sec. II C. The possibility of $E2$ transitions from the $3d$ levels of high-Z muonic atoms has been investigated and found to be negligible.[36]

It is easy to drop assumption (2) and to refine the estimates of intensity ratios by using correct relativistic wave functions, i.e., distinguishing the doublet members, and by allowing for differences in transition energies due to fs splitting. Energy differences due to hfs splitting may be neglected throughout.

C. Fine-Structure Intensity Ratios in Bi and Pb

Including the refinements discussed at the end of Sec. II B, one predicts for $Z\approx 80$ intensity ratios $K\alpha_1/K\alpha_2=1.92$, and $L\alpha_1/L\beta_1=1.75$. These ratios have not always been borne out by experiment; the ratios

[32] K. W. Ford and J. G. Wills, Nucl. Phys. **35**, 295 (1962).
[33] Professor V. L. Telegdi has pointed out the inconsistency in treating the single proton nonrelativistically, while treating the muon relativistically, for in Bi^{209} their velocities are quite comparable. He has suggested that the problem should be treated as a two-body interaction between proton and muon, operating in the field of the Pb^{208} core.
[34] K. Ford and J. G. Wills, Los Alamos Scientific Laboratory Report No. 2387 (1960) (unpublished).
[35] H. E. White and A. Y. Eliason, Phys. Rev. **41**, 753 (1933).
[36] H. L. Acker, G. Backenstoss, C. Daum, J. C. Sens, and S. A. DeWit, Nucl. Phys. **87**, 1 (1966).

TABLE II. Bi and Pb muonic x-ray intensity ratios.

		Acker *et al.*[a]	Anderson *et al.*[b]	Bardin *et al.*[c]	This experiment	Theory
Pb^{206}	$K\alpha_1/K\alpha_2$	1.45±0.10	2.0±0.3	···	1.72±0.10	1.92
	$L\alpha_1/L\beta_1$	1.57±0.15	1.8±0.3	···	1.42±0.22	1.75
Pb^{207}	$K\alpha_1/K\alpha_2$	···	···	···	1.75±0.15	1.92
	$L\alpha_1/L\beta_1$	···	···	···	1.56±0.34	1.75
Pb^{208}	$K\alpha_1/K\alpha_2$	···	···	···	1.68±0.18	1.92
	$L\alpha_1/L\beta_1$	···	···	···	···	1.75
Nat. Pb	$K\alpha_1/K\alpha_2$	1.50±0.15	1.8±0.3	···	1.65±0.14	1.92
	$L\alpha_1/L\alpha_1$	1.57±0.20	1.9±0.3	···	···	1.75
Bi^{209}	$K\alpha_1/K\alpha_2$	1.31±0.20	···	1.38±0.1	1.45±0.13	1.92
	$L\alpha_1/L\beta_1$	1.44±0.20	···	1.50±0.1	1.69±0.30	1.75

[a] Reference 36. [b] Reference 37. [c] Reference 9.

observed for Bi and Pb in recent experiments[9,36,37] (including this work) are summarized in Table II.

While the observed ratios for Pb are in rough agreement with the predicted values, Bi shows a marked anomaly, especially in the K doublet. This anomaly was first reported by Frati and Rainwater[18] (who found $K\alpha_1/K\alpha_2=1.33\pm0.09$ with a NaI detector and) who put forth the hypothesis of a nuclear "resonance" phenomenon to explain their observation. More specifically, they suggested that the muonic fs splitting coincides (at least roughly) with the excitation energy of a nuclear state of suitable spin and parity, so that the dynamic electric quadrupole hf coupling[38,39] is effective in mixing the fs components and leaving the Bi nucleus in that excited state. Rolnick,[40] however, explored this hypothesis quantitatively and concluded that it could not explain the results.

Hüfner[20] suggested the possibility of a different "resonance" effect to explain the anomalies. He postulated that the separation of the $3d_{5/2}$ and $2p_{1/2}$ muon levels (which are not connected by an allowed atomic transition) coincides accidentally with the excitation of a $\frac{15}{2}^+$ level in Bi (which has a $\frac{9}{2}^-$ ground state), and that the mixing occurs by $E3$ coupling. Hence the population of the $3d_{5/2}$ level (and, consequently, of the $2p_{3/2}$ to which it decays by $L\alpha_1$) is depleted, and that of the $2p_{1/2}$ enhanced, while the nucleus is left in the excited $\frac{15}{2}^+$ state at the end of the cascade. Figure 3 shows the intensity ratios predicted with this mechanism as a function of the percentage ratio ($\frac{15}{2}^+$ de-excitation gammas)/($L\alpha_1$ muonic x rays), i.e., of the fraction β of $d_{5/2}$ muons that lead to the excitation of the $\frac{15}{2}^+$ state. An entirely similar $E3$ "resonance" mixing can occur between the $3d_{5/2}$ and $2p_{3/2}$ levels if a suitable nuclear state with an excitation energy close to their separation exists. This mixing would, however, with currently available spectrometer resolutions, not lead to anomalous intensity ratios as the nuclear de-excitation γ ray would be confused with the $3d_{5/2}\rightarrow 2p_{3/2}(L\alpha_1)$ transition which it "replaces." On the other hand, the additional splittings that such a mixing would cause in some of the hfs substates of the $3d_{5/2}$ level could affect the hfs of the $L\alpha_1$ and $K\alpha_1$ lines.

Specifically, the hfs components of the $3d_{5/2}$ muon state become as a result of these two mixings:

$$\begin{aligned} &F=7: \quad \Psi=c_1|3d_{5/2}\rangle|\tfrac{9}{2}^-\rangle+c_2|2p_{1/2}\rangle|\tfrac{15}{2}^+\rangle, \\ &3\leq F\leq 6: \quad \Psi=d_1{}^F|3d_{5/2}\rangle|\tfrac{9}{2}^-\rangle+d_2{}^F|2p_{3/2}\rangle|\tfrac{9}{2}^+\rangle, \end{aligned} \tag{27}$$

whereas the $F=2$ component remains unchanged.

A comparison of the most recent information on the relevant nuclear[41] and muonic energy levels[9,35] is presented in Table III. As can be seen from this, both a $\frac{15}{2}^+$ and a $\frac{9}{2}^+$ Bi level exist which satisfy the requirement of the preceding discussion. Hüfner[42] has further shown that the relevant $E3$ matrix elements can easily have the requisite magnitudes.

Direct experimental evidence for the muonic excitation of these Bi levels is at present still incomplete. In our preliminary communication[43] we have reported the observation of a 1616-keV transition; this may be

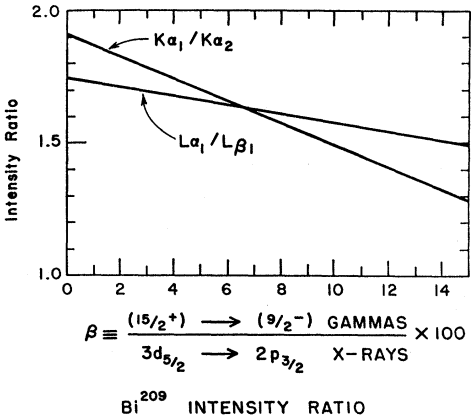

FIG. 3. Plot of K and L intensity ratios for Bi^{209} as a function of β, the fraction of $L\beta_1$ x rays missing due to the $E3$ mixing of the $15/2^+$ nuclear level.

[37] H. L. Anderson, R. J. McKee, C. K. Hargrove, and E. P. Hincks, Phys. Rev. Letters **16**, 434 (1966).
[38] B. Jacobsohn, Phys. Rev. **96**, 1637 (1954).
[39] L. Wilets, Kgl. Danske Videnskab. Selskab, Mat.-Fys. Medd. **29**, No. 3 (1954).
[40] W. B. Rolnick, Phys. Rev. **132**, 1110 (1963).
[41] J. C. Hafele and R. Woods, Phys. Letters **23**, 579 (1966).
[42] J. Hüfner, Phys. Letters **25B**, 189 (1967).
[43] Ehrlich *et al.* (Ref. 1).

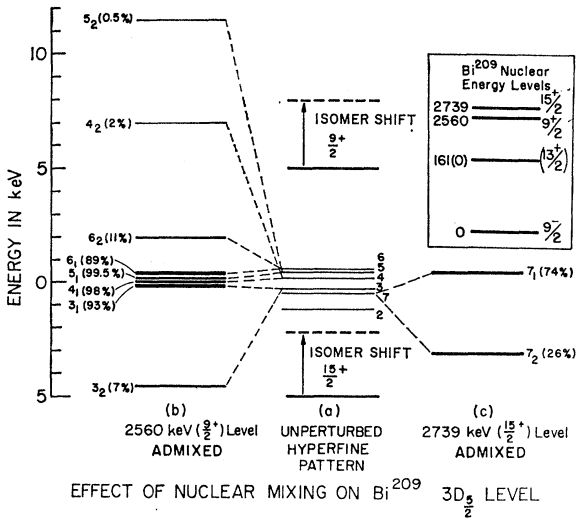

FIG. 4. Effects of the $E3$ mixing of the $9/2^+$ and $15/2^+$ levels on the $3d_{5/2}$ muon levels. (a) the six levels in the center are the unperturbed components of the $3d_{5/2}$ level, each labeled with its own F. The heavy line below marked with $15/2^+$ indicates the approximate energy separation between the original $15/2^+$ nuclear level and the $3d_{5/2}$ components; the dashed line indicates the approximate separation of these levels due to the isomer shift. The pair of lines above the six levels indicate the same quantities for the $9/2^+$ level, where the nuclear level ($3d_{5/2}$) is measured relative to the ground state (center of gravity of the $2p_{3/2}$). (b) and (c) each show the split levels, with the percentage of nuclear ground-state intensity indicated in parentheses. The component containing more than 50% nuclear ground state is labeled with subscript 1; the component which is mostly excited state is labeled with subscript 2. In the upper right-hand corner are displayed the relevant nuclear energy levels in Bi.

identified with a $\frac{13}{2}^+ \rightarrow \frac{9}{2}^-$ (g.s.) transition. More recent data[44] indicate the presence of a 1134-keV line (identified as $\frac{15}{2}^+ \rightarrow \frac{13}{2}^+$ transition of interest). This latter transition thus would correspond to the first resonance entry in Table III.

The question most germane to our work is: Do these resonances affect the observed hfs and its interpretation? A cursory study of the problem based on all available estimates of the pertinent parameters indicates that such effects would be minor ($\sim 10\%$).

We shall discuss this question with reference to Fig. 4:

(1) The nuclear mixing of the $3d_{5/2}$ and $2p_{1/2}$ levels (via the $\frac{15}{2}^+$ state) leads to the following effects:

(a) The $F=7$ hf component of the $3d_{5/2}$ level is split into two components [7_1 and 7_2 in Fig. 4(c)]. Taking the observed value[44] of the parameter β as 0.1 and Hüfner's[42] value of 1.8 keV for the $E3$ matrix element, we infer that the energy difference between the unperturbed $F=7$ states that are mixed, i.e., $|3d_{5/2}\rangle|\frac{9}{2}^-\rangle$ and $|2p_{1/2}\rangle|\frac{15}{2}^+\rangle$, is $\Delta E=2$ keV. Such a value of β implies that the $K\alpha_1/K\alpha_2$ and $L\alpha_1/L\beta_1$ intensity ratios are 1.49 and 1.58, respectively, values which are consistent with all data (see Table II). The $E3$ mixing produces a splitting of the $F=7$ component of the unperturbed $3d_{5/2}$ level of ~ 4.1 keV and the new eigenstate 7_1 contains a 26% (intensity) admixture of the $|2p_{1/2}\rangle|\frac{15}{2}^+\rangle$ state.

(b) The 7_1 and 7_2 states are fed from the $4f$ states in proportion to their d-state contents, and attain their proper mixed composition after they have been populated before they further cascade. Thus the total d-state content of these states will be $0.62=(0.26)^2+(0.74)^2$, as compared to 1 in the absence of mixing. This fact in turn reduces the population of the $F=6$, $2p_{3/2}$ level by 0.29.

(c) The muon in $2p_{1/2}$ and $1s_{1/2}$ states with the nucleus in the $\frac{15}{2}^+$ excited state may experience

(i) an isomer shift due to a difference in the sizes of the two states, and

(ii) $M1$ hfs splittings different from those arising with the nucleus is in its ground ($\frac{9}{2}^-$) state.

Consequently, the hfs of the $K\alpha_1$, $K\alpha_2$, and $L\alpha_1$ transitions will be affected by the mixing caused by the $\frac{15}{2}^+$

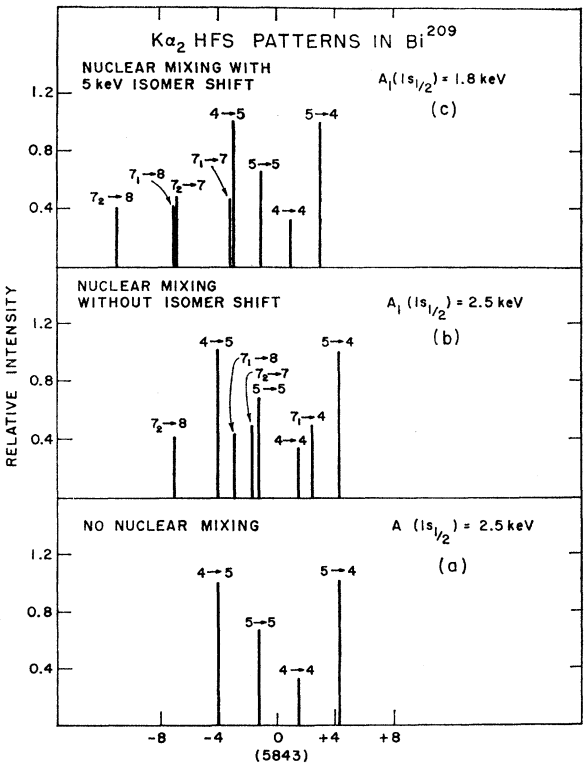

FIG. 5. Line spectra of $K\alpha_2$ for (a) no nuclear mixing, (b) nuclear mixing without isomer shift, and (c) nuclear mixing with a 5-keV isomer shift; it should be remembered that the radiative width of each line is about 1 keV. The numbers above each line indicate the initial and final values of F. Although these spectra are illustrative, they are drawn for the hf constants which give the best χ^2 to the data (see Sec. IV E). The energy of the unperturbed transition is taken as zero; the observed center of gravity energy (in keV) is indicated in parentheses.

[44] C. K. Hargrove (private communication); H. L. Anderson, M. S. Dixit, H. J. Evans, D. Kessler, R. J. McKee, R. Barton, C. K. Hargrove, E. P. Hincks, and J. McAndrew (to be published).

TABLE III. Nuclear transitions in Bi^{209} in possible resonance with muonic transitions (keV).

	Nuclear transitions		Muonic transitions
$15/2^+ \rightarrow 9/2^-$:	2739[a]±3		2747±3.9[c]
		$3d_{5/2} \rightarrow 2p_{1/2}$[b]:	2749±3.6[d]
			2744.3[e]
$9/2^+ \rightarrow 9/2^-$:	2560[a]±3		2554.8±2.0[c]
		$3d_{5/2} \rightarrow 2p_{3/2}$:	2556.6±2.5[d]
			2553.6[e]

[a] Reference 41.
[b] The energy of the forbidden ($3d_{5/2} \rightarrow 2p_{1/2}$) transition is obtained by adding the energy of the ($3d_{5/2} \rightarrow 2p_{3/2}$) transition to the observed $2p$ fine structure splitting.
[c] Reference 36.
[d] This work.
[e] Reference 9.

(2739 keV) state. In Fig. 5 we show the theoretical line spectra of the $K\alpha_2$ transition for the three cases discussed in Sec. IV E. We chose the hf constants, anticipating the results of Sec. IV E, which yield the best χ^2.

(2) The mixing of the $3d_{5/2}$ and $2p_{3/2}$ levels produces the following effects:

(a) The $F=3, 4, 5$, and 6 hfs components of the $3d_{5/2}$ level are each split into two components (see Fig. 3). It should be stressed that the resonance here is so sharp that the hfs of the $2p_{3/2}$ level *is important in determining the extent of the mixing.* In our estimates we have retained Hüfner's[42] values for the $E3$ matrix elements, and assumed (see Table III) an energy difference of -5 keV between the muonic levels (unperturbed by normal hfs) and the $\frac{9}{2}^+$ nuclear level. We find that the mixed hf states attain the $3d_{5/2}$ contents indicated in Fig. 4(b).

(b) The $2p_{3/2}$ and $1s_{1/2}$ states again exhibit isomer shifts and altered $M1$ hf interactions.

In conclusion, only the hfs of the $K\alpha_2$ and $L\alpha_1$ transitions will be affected by the admixture of the $\frac{9}{2}^+$ (2500 keV) state. In Fig. 6 we show the theoretical line spectra of the $K\alpha_1$ transition for the three cases discussed in Sec. IV E. In the above calculations we have assumed that $E2$ and $M1$ interaction constants of the excited states ($\frac{15}{2}^+$, $\frac{9}{2}^+$) are of the same order as those of the ground state ($\frac{9}{2}^-$).

TABLE IV. Physical properties of Pb isotope targets.

Isotope	Dimensions (cm)	Weight (g)	% isotope composition 206	207	208
207	7.0× 7.0×0.32	384.5	2.2	92.4	5.5
207	7.0× 7.0×0.64	96.4	2.5	92.9	4.7
206	7.0× 7.0×0.95	540	88	9	3
206	5.3× 5.3×0.64	219	88	9	3
208	5.4× 5.4×0.95	117.4	0.2	0.05	99.8
208	5.4× 5.3×0.32	76.2	0.2	0.05	99.8
Nat. Pb	15.2×15.2×1.0	2540	24.9	21.4	52.3

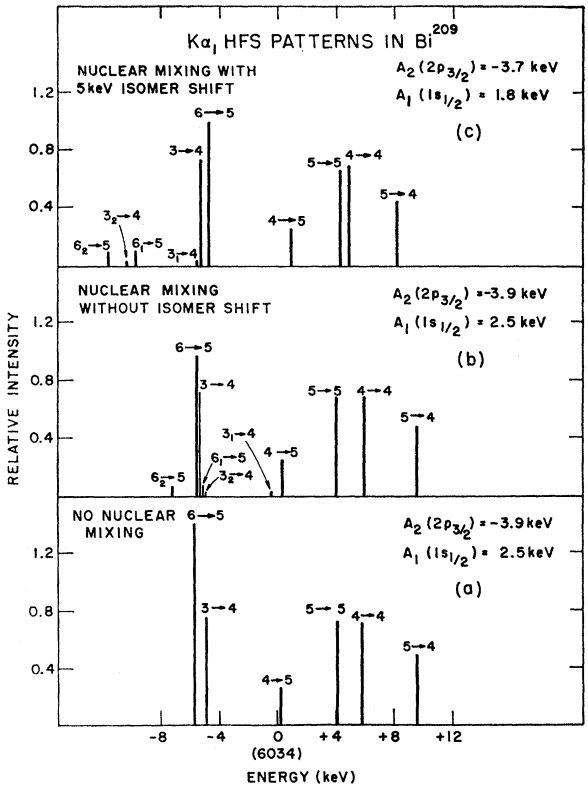

FIG. 6. Line spectra of $K\alpha_1$ hfs for (a) no nuclear mixing, (b) nuclear mixing without isomer shift, and (c) nuclear mixing with a 5-keV isomer shift. The notation is the same as in Fig. 5.

In Sec. IV E, we shall discuss sensitivity of our data to these effects and the influence of the latter on the inferred values of the hf constants A_1 and A_2.

III. EXPERIMENTAL APPARATUS AND PROCEDURE

A. Muon Stops Telescope

The counter arrangement, pictured in Fig. 7, was quite conventional. Counters 1, 2, and 4 defined the beam. (1,2) coincidences were used as a beam monitor. The Čerenkov counters 3 and 3′ served to veto electrons. A graphite moderator of 4.7 g/cm² in front of counter 3 was used to reduce the velocity of the incoming muons below their Čerenkov threshold. Brass shielding between counters 3 and 3′ confined the beam to a 15×15 cm² area. An additional brass moderator was inserted between counters 3′ and 4 to bring the peak of the muon range curve into the targets.

Immediately behind counter 4 was a square array of four identical 10×10 cm² counters T_i ($i=1,2,3,4$). Each of these counters intercepted essentially $\frac{1}{4}$ of the beam. Since each counter was electronically independent of the others, we thus had essentially four independent (but labeled) stopping beams; this allowed us to observe muonic x rays from four targets *simultaneously.*

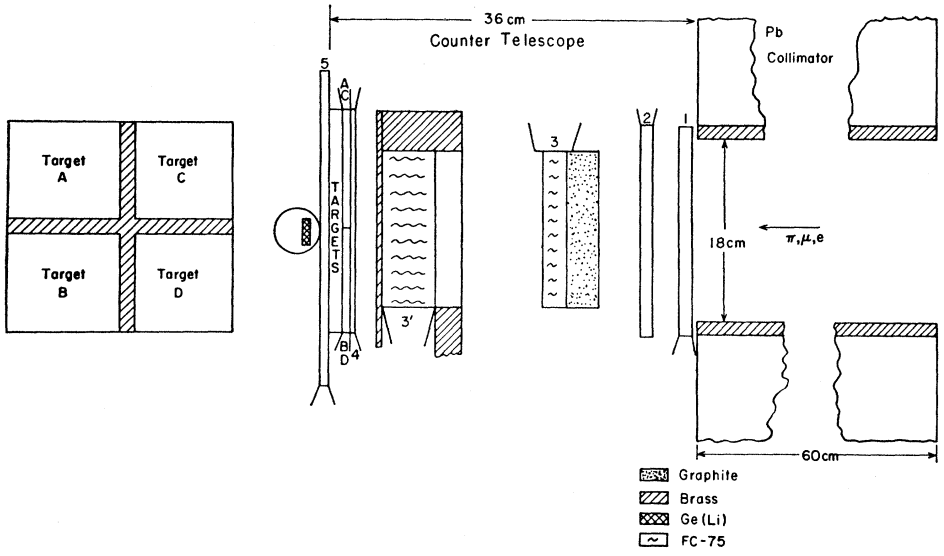

FIG. 7. Physical arrangement of apparatus. A muonic x-ray event which was analyzed is given by $(24T_i)\sim(3,3'5)X$; a calibration event, $\sim(3,3'5)X$. ($\sim$ means "not.") Counters 1 (20×20×1 cm), 2 (20×20×1 cm), 4 (20×20×1 cm), T_i (10×10×0.6 cm), and 5 (30×30×1 cm) were plastic scintillators. The Cerenkov counters, 3 (15.2×15.2×2.5 cm) and 3′ (15.2×15.2×5.1 cm), were filled with FC-75. The Ge(Li) was placed in the beam directly behind counter 5.

Such a comparative procedure was first described by a group at Columbia.[45]

The targets, whose relevant physical properties are given in Table IV, were placed between the counters T_i and counter 5, and separated from each other by a cross-shaped brass absorber. A $(24T_i)\sim(3,3'5)$ coincidence (where $\sim$ means "not") defined a muon stop in the target i behind counter T_i. The muon-stop coincidences were purposely broad ($\sim$600 nsec), and will be discussed more thoroughly in the next section. Typical rates were 5×10^3 stops/sec g/cm^2 in the 15×15 cm^2 target area.

A test of how well the targets were electronically separated from one another is provided by a comparison of the K x ray spectra of Pb^{206} and Bi^{209} in Fig. 8, which were taken simultaneously; no feed-through between the targets is detectable.

The Ge(Li) detector X was a cylinder 19 mm in diam and 13.7 mm deep with a dead layer of less than $\frac{1}{4}$ mm on the circular face. This crystal, whose circular sides faced into the beam, was placed directly behind counter 5, essentially at the midpoint of the target array. Its position was so adjusted that it saw approximately equal

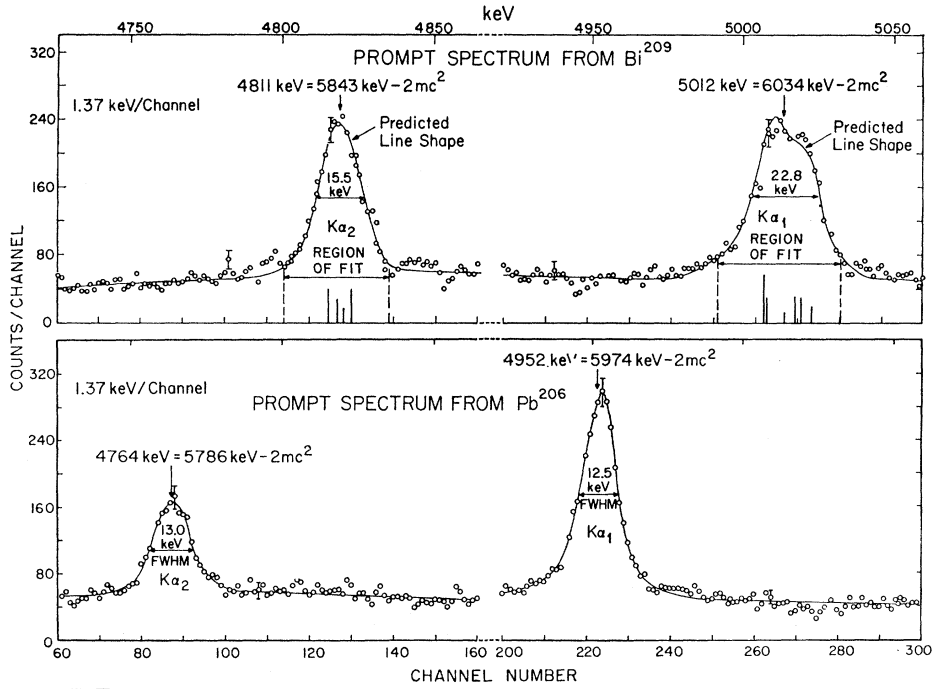

FIG. 8. Comparison of muonic K x rays in Bi^{209} and Pb^{206}. The line spectra shown at the base line are the hfs patterns calculated with the parameters which yield a minimum χ^2, assuming no nuclear mixing (see Table IX). The solid line represents the theoretical predictions normalized in the regions of fit and obtained by folding the observed Pb^{206} $K\alpha_1$ line shape (corrected for isotopic contamination).

[45] R. C. Cohen, S. Devons, A. D. Kanaris, and C. Nissim-Sabat, Phys. Letters **11**, 70 (1964).

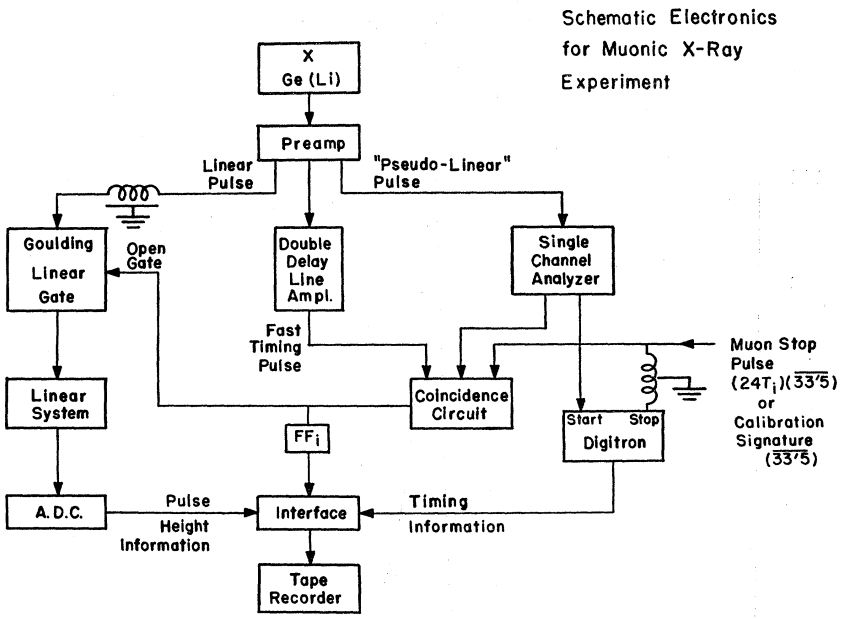

FIG. 9. Electronic schematic diagram showing the logic associated with a typical event (either a stop in target i or a calibration event). A broad coincidence is made between the "fast timing pulse," the "psuedo-linear pulse" (which has been energy selected by the single-channel analyzer), and a muon stop (or calibration signature). This broad coincidence sets a flip-flop and opens the Goulding linear gate, which allows the linear pulse to be amplified in the linear system and analyzed in the ADC. Digitron is started by the pseudolinear pulse and stopped by a muon stop (or calibration signature). The tape interface then reads out the pulse height, timing, and flip-flop number and writes the information on magnetic tape, one event at a time.

count rates from all four targets. The rate of pulses with heights greater than 500 keV was typically 7.5×10^3/sec.

B. Electronics

Essentially, two-parameter spectra were collected and stored on magnetic tape. For each event the pulse height, the target number, and the time interval between the muon stop and x ray were recorded.

Figure 9 is a schematic diagram of the electronic logic for a typical event (either a stop in target i or a calibration event). Actually, five independent coincidences are made. Pulses from X went directly to a preamplifier[46] which provided pulse shaping and a charge gain of 2×10^{-12} V/C, and from which three identical pulses were derived. One of these, called the *linear pulse*, was fed through a linear amplification system into the ADC of a commercial 400-channel (RIDL Model 34-12) pulse-height analyzer (PHA). The two other outputs were used to perform logical decisions related to the analysis of the linear pulse. One called the *pseudolinear pulse* was sent to a single-channel analyzer. The other, the *fast-timing pulse*, went[47] to a double-delay line amplifier which produced a narrow (about 10 nsec) and essentially jitter-free (<2 nsec over the energy range set by the single-channel analyzer) timing pulse.

In the linear branch, the preamplifier was followed by a normally closed Goulding-type[48] linear gate. This gate, with a dynamic range of 10 V, was opened by events giving a muon-stop signature and lying within an energy window set by a single-channel analyzer; its purpose was to protect the main amplifier (recovery time 2 msec) from the high rates present in X.

The linear system consisted of a biased main amplifier (a modified Ortec 203) and a pulse stretcher. The modifications of the biased amplifier included supplying all filaments from external dc supplies. The pulse stretcher shaped the linear pulses for analysis by the PHA. The entire linear amplification system, except for the preamplifier, was kept inside a thermostatted cabinet that maintained the temperature constant to within ±0.2°C; the ambient temperature was constant to within 2°C. The gains and biases were so adjusted that the energy regions of interest for the observation of 2-quantum escape peaks (4400–5200 keV for the K x rays, 1200–2000 keV for the L x rays) covered the 400 channels of the PHA. As a result of the temperature controls, drifts in the spectra were generally less than 0.5 keV over periods of a few hours.

Fast electronics[49] was used to generate the pulse that opened the Goulding gate; this pulse was essentially generated by a coincidence between the fast-timing pulse, and the output of the single-channel analyzer. These gating pulses, defined as "events," were 600 (400) nsec wide when $K(L)$ muonic spectra were collected. The linear pulse was delayed about 300 (200) nsec before the Goulding gate, so that prompt events arrived there about 200 nsec after it had been opened. This timing arrangement enabled us to observe accidentals as uncorrelated "early events"; this point will be discussed in the next section.

[46] Model No. PASD1-45, designed by I. S. Sherman of the Electronics Division, Argonne National Laboratory.

[47] T. K. Alexander and G. C. Nielson, in Proceedings of the Conference on Instrument Techniques in Nuclear Pulse Analysis, Monterey, Calif., 1963 (unpublished).

[48] F. S. Goulding, Lawrence Radiation Laboratory, University of California, Berkeley, Model 11X1431 T-1.

[49] A. Barna, J. H. Marshall, and M. Sands, Nucl. Instr. Methods 1, 124 (1960; California Institute of Technology Report No. CTSL-17 (unpublished); A. Barna and J. H. Marshall, California Institute of Technology Synchrotron Laboratory Report No. CTSL-18 (unpublished).

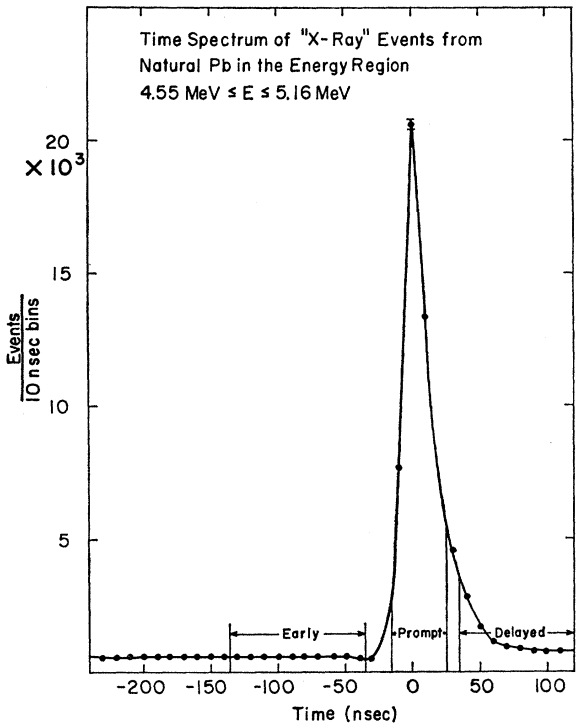

FIG. 10. Time spectra of events in Pb K energy region. The region marked "early" contains events uncorrelated to the muon stop; the region marked "prompt" includes events related to simultaneous muon stops such as muonic x rays and prompt backgrounds; the region marked "delayed" contains delayed correlated events such as capture gammas as well as events uncorrelated to the muon stop.

Each time an event occured, a flip-flop corresponding to a specific target T_i was set and remained set until the event was analyzed and recorded. A fifth category of events, called calibration events, included all those pulses in X which had the appropriate pulse height but were in anticoincidence with the beam. This category included calibration pulses which were applied to the input of the preamplifier, as well as pulses in X produced by radioactive sources. Calibration events also set a flip-flop which remained set until the data were recorded.

Once an event had occurred, a blocking gate (not shown in Fig. 9) prevented the Goulding gate from being opened again until this blocking gate received a signal from the tape unit indicating that the data had been recorded.

C. Digitron

A digital instrument, functionally identical to the "digitron" described by Lundy,[50] was used to measure the time interval between the muon stop (or calibration signature) and a pulse from the preamplifier, which satisfied certain criteria. Specifically, this pulse had to be passed by the single-channel analyzer and be in anticoincidence with a traversing beam particle. We used the standard procedure of running the digitron "backwards," starting it with an energy-selected pseudolinear pulse (less than $\frac{1}{10}$ the muon-stop rate) and stopping it with the delayed muon-stop (or calibration) signature.

Figure 10 shows as an example a typical timing curve for events in the Pb K x-ray energy region. To the left of the prompt peak, one sees early events, i.e., pulses in X which preceded the muon stops. These events are uncorrelated and hence constitute an accidental background. To the right of prompt peak one sees the delayed events; these may or may not be correlated. Gamma rays from the products of muon capture, a process which occurs with high probability in heavy nuclei, will yield correlated delayed events distributed exponentially in time with a mean life characteristic of the target. Our two-parameter (pulse-height–time) spectra enable us to separate our data using time or energy criteria: We can enhance the quality of capture γ spectra by selecting the appropriate time regions. These capture γ's are useful for energy calibration and for line-shape study purposes. Furthermore, accidental and capture γ events are taken simultaneously with the muonic x-ray data, thus avoiding certain systematic normalization problems. This method, however, does not enable one to determine prompt backgrounds. A comparison of prompt and delayed spectra from Bi, showing the 2.615-MeV γ ray of Pb^{208}, is given in the bottom of Fig. 11.

D. Procedure for Collecting Data

Individual x-ray runs generally lasted 1 h. During each run, pulses from a 60-cps precision mercury pulser were injected into the linear system for periods of about 1.5 sec, at intervals of about 50 sec. Specifically, the voltage supply of this pulser was fed through a relaxation oscillator which was nonconducting except during the interval just specified. This "burst generator" also produced, during its operation, a level which opened the normally closed calibration event gate. At the beginning and end of each run, the dc voltage of the pulses was measured (to within 1 part in 10^5) with a vacuum-tube differential voltmeter. If it had changed during the run, it was readjusted. Such changes were typically of the order of 2/75 000, corresponding to an energy drift of $\sim$0.4 keV in the K region.

A 15-min calibration run with radioactive sources was made every few hours with the beam on but in anticoincidence. The calibration lines used were

(1) the full-energy, 1-quantum, and 2-quantum escape peaks produced by the 6.130-MeV γ from O^{16*};

(2) the 2-quantum escape of the 2.6145-MeV γ from ThC″;

(3) the full-energy peak of the 1.332-MeV γ from Co^{60}.

[50] R. A. Lundy, Rev. Sci. Instr. 34, 146 (1963). The present Digitron, using integrated circuits, was designed by T. A. Nunamaker of this Institute.

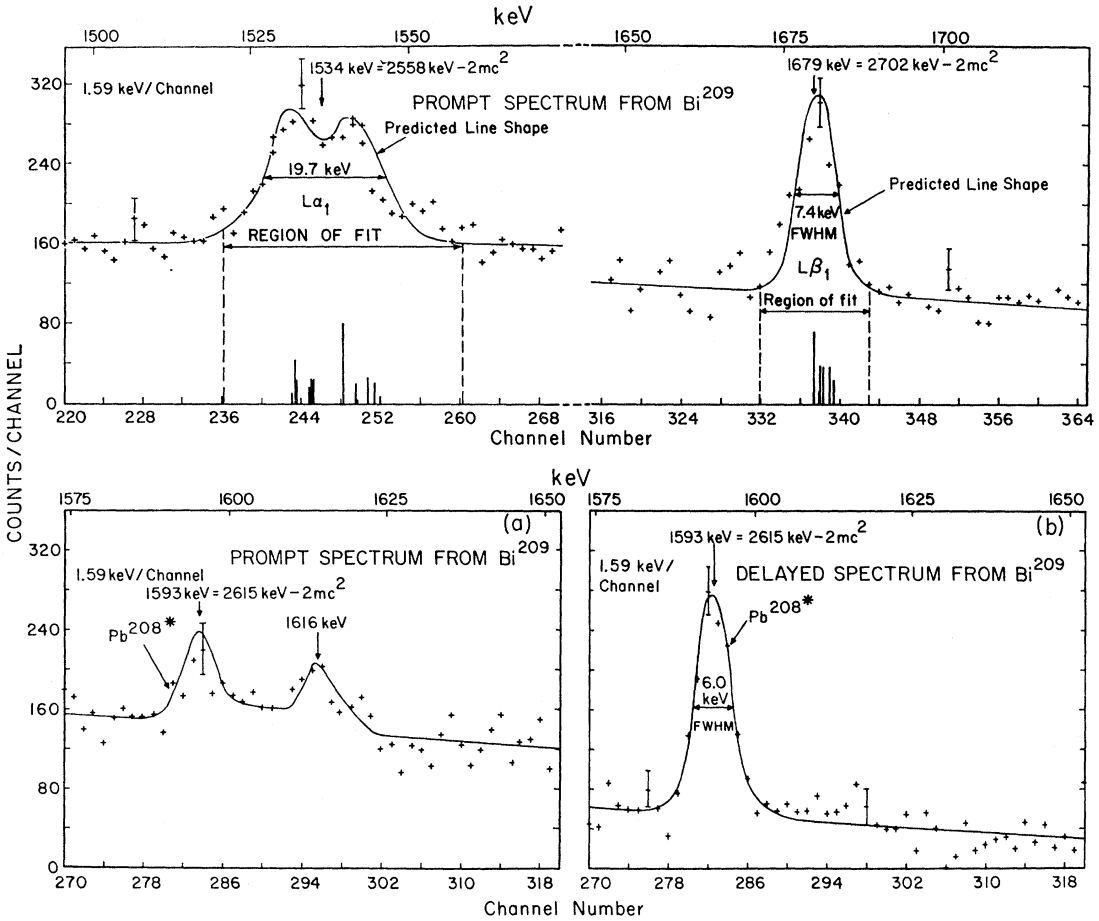

FIG. 11. (Top) Muonic L x-ray spectrum from Bi^{209}. The line patterns calculated with the parameters for an extended dipole listed in Table IX (assuming no nuclear mixing). The solid line represents the theoretical predictions normalized in the region of fit and obtained by folding in the observed line shape of the 2.615-MeV γ ray from Pb^{208}. (Bottom) Delayed (a) and prompt (b) spectra in the energy region between the two Bi L lines. The time window (with respect to the muon stop) is -15 to $+25$ nsec for the prompt events, and $+35$ to 145 nsec for the delayed events.

The over-all linearity of the amplification system was determined by measuring the PHA channel number as a function of the pulser input voltage given by the differential voltmeter. A least-squares fit of a straight line to a differential linearity curve taken in conjunction with the Pb K isotope run showed a maximum variation of channel width of $\pm 5\%$ from the mean.

An important part of data collection involves the determination of backgrounds. In Sec. III C, we commented on the nonprompt backgrounds, which can be separated from the real events on the basis of time information.

We determined prompt backgrounds, for which this separation is not possible, by replacing the standard targets by lower Z dummies of the same stopping power. These targets were so chosen that their muonic x rays could contribute only a negligibly few events in the energy regions of interest; at the same time, they were to have the highest possible Z, so as to approximate the radiative properties of the real targets. A Ta target satisfies these criteria in the Bi and Pb K x-ray energy regions; while the full-energy peaks of its K x rays do fall in the selected energy region, they are nearly two orders of magnitude smaller than the 2-quantum escape peaks. We found that about 34% of the flat background of the Bi and Pb spectra was contributed by prompt events. Similarly, using a Ti dummy target, which has practically no x-ray events about 1.5 MeV, we found that about 83% of the flat background in the Bi and Pb L regions was due to this source. These prompt events were probably due to bremsstrahlung produced by electrons (primarily from muon decay) in the targets and the various absorbers.

IV. DATA ANALYSIS AND RESULTS

A. Operations of Analysis

The analysis of the data consisted of three major steps: (1) combining the spectra from individual runs,

TABLE V. 5-parameter fits of Lorentzian shape to Pb isotope K data.

		χ^{2a}
Pb^{208}	$K\alpha_1$	35
	$K\alpha_2$	33
Pb^{207}	$K\alpha_1$	31
	$K\alpha_2$	20
Pb^{206}	$K\alpha_1$	35
	$K\alpha_2$	20

[a] For 26 deg of freedom.

(2) subtracting background, and (3) extracting the pertinent parameters.

Step (1) involved two operations: correcting (a) for drifts, and (b) for nonlinearities in the gain of the electronics. The first of these corrections was straightforward, since the periodically injected calibration pulses (see Sec. III D) provided a running safeguard against drifts as well as a record if they occurred. Using this information, we shifted the individual runs to maintain the centroids of the calibration peaks in the same channel to within 0.1 channel (0.15 keV); note that while we used a 400-channel PHA, our system was equivalent to a 3400-channel analyzer with its first 3000 channels biased off. This shifting assumes that the drifts were caused by shifts in bias levels rather than to absolute gain changes. Had these drifts been due exclusively to changes in gain, the error in gain between individual runs would have been at most 0.1 keV over the relevant energy region, since the maximum excursions of the pulser centroid were less than 1 part in 5000.

The correction for the differential nonlinearity of the gain involved folding an empirical dispersion (keV/channel) curve into raw data, so as to make all channels equally wide in energy. A least-squares fit of a straight line to the differential linearity curve for measurements

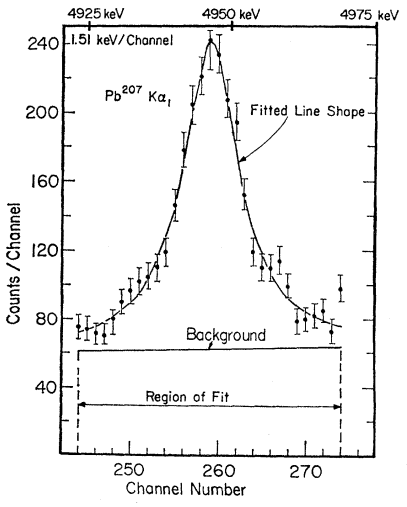

FIG. 12. Least-squares fit of a Lorentzian line shape to the Pb^{207} $K\alpha_1$. The fitted parameters are the height, width, and centroid of the Lorentzian and a linear background. The χ^2 was 31 for 26 deg of freedom.

taken before and after the Pb K isotope data showed that the maximum deviation of channel width from the average was no more than 5%. There appeared to be a slight systematic upward shift of the dispersion curve during the collection of data, but this effect amounted to an ambiguity of at most 0.2 keV over a region of 200 keV, i.e., over the largest energy difference of interest in our spectra. In the isotope-shift measurements, this effect was of the order of 0.01 keV.

We have already discussed the subtraction of backgrounds, both prompt and noncoincident. We shall defer the details of the extraction of the parameters to the sections covering the pertinent results.

B. Results: Pb Isotope Shifts and Bi-Pb Isotone Shifts

In a preliminary analysis of the isotope-shift data, we attempted to use a straightforward centroid calculation. This method proved, however, to be unsatisfactory inasmuch as the derived centroids of the peaks were too sensitive to the choice of the spectral region used in the analysis. We therefore turned to another method, viz., fitting assumed line shapes to the data.

Both Gaussian and Lorentzian line shapes were tried. These shapes were suggested by the remarkably symmetric observed peaks; their use was justified *a posteriori* by the goodness of the fits (χ^2) obtained with them. It was found that the Lorentzian shape gave, in general, slightly better fits, but in all cases both line shapes gave the same centroids. These fits involved five parameters, viz., the position, height, and width of the peak, as well as the slope and mean height of the background, and were made with the constraint that the number of counts in experimental and theoretical spectra be the same. Figure 12 shows a typical fit to an observed line.

In Table V are listed the χ^2's for the Lorentzian fits to the Pb K isotope data. These fits were taken over 31 channels, but comparison with fits taken over 71 channels produced discrepancies which were typically only 0.05 channels ($\sim$0.08 keV). A more thorough discussion of errors follows.

Since data used in relative measurements were taken simultaneously, the effect of many sources of systematic error, e.g., electronic instabilities and fluctuations in beam intensity and/or time structure, were cancelled. Checks had to be made, however, to show that no significant bias was introduced by keeping targets in fixed positions.

The most straightforward check was to use a single target which covered all four positions, and to look for asymmetries in the four individual spectra. Such a test, performed with a natural Pb target, yielded an average deviation of the $K\alpha_1$ centroids from the mean by 0.8 standard deviations, while for the $K\alpha_2$ centroids the average deviation was 1.2 standard deviations. The probability for this to be caused by purely statistical fluctuations is 43 and 23% for the $K\alpha_1$ and $K\alpha_2$ lines, respectively. We therefore deemed it necessary to

increase the errors of the isotope shifts to allow for the possibility of a systematic effect. This allowance proved to be the major contribution to the quoted error in the isotope shift.

Another source of systematic error was found in a calibration ambiguity. The precision pulser gave locally consistent readings when compared to a radioactive source but slightly inconsistent readings over energy regions as wide as 3 MeV. Since calibration sources were available in the region of the x rays, this caused no serious problem. The measurement most affected was the $2p$ fs splitting, where this effect caused an uncertainty of 2.0 keV. On the other hand, the effect on the Pb I.S.'s was less than 0.1 keV.

In Table VI we list our isotope-shift results. The quoted errors are standard deviations, augmented to allow for the possibility of positional asymmetries (see above). These standard deviations were obtained from the error matrix associated with the 5-parameter fit and allow for all of the correlations between the parameters. The I.S.'s have been corrected for isotopic contaminations.

Aside from this work, the only other muonic Pb isotope data in the literature is by Anderson *et al.*[37] They looked separately at muonic x rays from natural Pb and from Pb^{206}. By assuming the optical value[2] for the $(Pb^{206}\text{-}Pb^{207})/(Pb^{206}\text{-}Pb^{208})$ I.S. ratio they inferred the $Pb^{206}\text{-}Pb^{208}$ I.S. More recently, using techniques entirely similar to ours, they obtained data[4a,51] which are in excellent agreement with the present results.

We include in this section a discussion of the $Pb^{208}\text{-}Bi^{209}$ isotone shift (It.S.), because the experimental technique was the same as the I.S., although the final accuracy was considerably less. We actually measured the shifts between the K and L transitions of Pb^{206} and Bi^{209} (Table VII). The major source of error in these measurements was the calibration ambiguity mentioned above. We are not aware of any other simultaneous measurements of Pb and Bi, and we find it difficult to assess the errors of measurements taken separately; therefore, we have not listed any other It.S. measurements for comparison in Table VII. It is clear from the absolute-energy measurements of other groups that our results are consistent.

Combining the above shift with our $Pb^{206}\text{-}Pb^{208}$ I.S., we find for the $Bi^{209}\text{-}Pb^{208}$ It.S. the values

$$\begin{aligned}\Delta K\alpha_1 &= 69.3\pm2.0 \text{ keV},\\ \Delta K\alpha_2 &= 63.5\pm2.2 \text{ keV}.\end{aligned} \tag{28}$$

C. Results: Absolute Transition Energies of Pb^{206} and Bi^{209}

Although the primary purpose of this experiment was not to measure absolute energies, we present for completeness a comparison of our results (Table VII) with those of other recent Ge(Li) measurements. Absolute region measurements in the K energy region are no longer seriously affected by the uncertainty of the energy of the nuclear γ ray from the 3^- level in O^{16} to the ground state. Within the past six months more precise values of this energy have been published, viz., 6127.8 ± 1.2 keV[52] and 6129.96 ± 0.43 keV.[53] The fact that we referenced our K x-ray data to the latter value explains why our errors appear smaller than those of others. Our major source of error is the calibration ambiguity (see Sec. II B).

TABLE VI. Muonic isotope shifts (keV).

		This expt.	Anderson *et al.*[a]
$Pb^{206}\text{-}Pb^{207}$	$K\alpha_1$	3.72 ± 0.32	···
	$K\alpha_2$	4.02 ± 0.86	···
$Pb^{206}\text{-}Pb^{208}$	$K\alpha_1$	9.36 ± 0.30	10.2 ± 1.4[b]
	$K\alpha_2$	9.27 ± 0.89	8.4 ± 1.4[b]
$Pb^{206}\text{-}Pb^{207}$	$L\alpha_1$	0.54 ± 0.62	···
	$L\beta_1$	1.31 ± 0.59	···

[a] Reference 37.
[b] Inferred from Pb^{206} and natural Pb data, assuming the optical $(Pb^{206}\text{-}Pb^{207})/Pb^{206}\text{-}Pb^{208})$ I.S. ratio.

All of the Bi energies relate to the centers of gravity of the hfs-broadened peaks.

There is on the whole acceptable agreement for the K lines and excellent agreement for the L lines. The latter fact is not surprising since one of the calibration lines (the 2614.5-keV Pb^{208} γ) falls between the $L\alpha_1$ and $L\beta_1$ peaks.

D. Results: Intensity Ratios in Pb and Bi

We now discuss the intensity ratios of the $K\alpha_1$, $K\alpha_2$, $L\alpha_1$, and $L\beta_1$ fs components. The observed ratios were corrected for the energy dependence of (1) the pair-production cross section in Ge, (2) the self-absorption in the target, and (3) the probability for the escape of secondary electrons. The total correction for the $K\alpha_1/K\alpha_2$ ratio is only -1%. In Pb, the $L\alpha_1/L\beta_1$ had to be corrected by $+14\%$ for (1), $+1\%$ for (2) and -1% for (3). The correction for Bi is the same.

Table II summarizes our intensity ratios for Bi and various Pb, as well as the most recent results obtained by other groups[9,36,37] with Ge(Li) spectrometers. We find no statistically significant difference between the intensity ratios from the different Pb isotopes, and these ratios in turn are consistent with the results from natural Pb. On the other hand, we measure systematically lower ratios than standard electromagnetic theory would predict.

Our results are in fair agreement with other measurements, with the glaring exception of the Pb^{206} $K\alpha_1/K\alpha_2$

[51] H. L. Anderson, in Proceedings of the International Conference on Electromagnetic Sizes of Nuclei, Ottawa, 1967 (to be published).

[52] R. E. Berg and E. Kashy, Nucl. Instr. Methods **39**, 169 (1966).

[53] C. Chasman, K. W. Jones, R. A. Ristinen, and D. E. Alburger, Phys. Rev. **159**, 830 (1967).

TABLE VII. Recent Pb and Bi muonic x-ray energies (keV).

		Acker *et al.*[a]	Anderson *et al.*[b]	Bardin *et al.*[c]	This experiment
Pb^{206}	$K\alpha_1$	5972.3 ±5.0	5979.7±5.2	···	5974.1 ±2.0
	$K\alpha_2$	5786.9 ±5.0	5792.1±5.0	···	5789.0 ±2.8
	$\Delta 2p$	185.4 ±2.0	187.6±1.4	···	185.1 ±2.0
	$L\alpha_1$	2500.6 ±1.5	2502.8±1.8	···	2503.4 ±2.3
	$L\beta_1$	2643.2 ±3.0	2645.1±1.9	···	2645.5 ±2.3
	$\Delta 2p$-$\Delta 3d$	142.6 ±2.5	142.3±1.4	···	142.1 ±1.7
Bi^{209}	$K\alpha_1$	6032.2 ±5.0	···	6032.3±3.0	6034.0 ±2.2
	$K\alpha_2$	5839.7 ±5.5	···	5841.6±3.0	5843.2 ±2.5
	$\Delta 2p$	192.5 ±2.0	···	190.7	190.8 ±2.5
	$L\alpha_1$	2554.8 ±2.0	···	2553.6	2556.1 ±2.5
	$L\beta_1$	2700.2 ±2.5	···	2700.6	2702.8 ±2.5
	$\Delta 2p$-$\Delta 3d$	145.4 ±2.0	···	147.0	146.7 ±2.0
Bi^{209}-Pb^{206}	$K\alpha_1$	···	···	···	59.9 ±2.0
	$K\alpha_2$	···	···	···	54.2 ±2.0
	$L\alpha_1$	···	···	···	52.7 ±2.0
	$L\beta_1$	···	···	···	57.3 ±2.0
Calibration values adopted	O^{16}	6131 ±4.0[d]	6130 ±4.0	6131 ±4.0	6129.96±0.43[e]
	ThC″	2614.47±0.05[f]	2614.5±0.1	2614.5±0.1	2614.47±0.05
	Co^{60}	1332.38±0.05[f]	1332.5±0.1	···	1332.38±0.05

[a] Reference 36.
[b] Reference 37.
[c] Reference 9.
[d] C. P. Browne and I. Michael, Phys. Rev. 134, B133 (1964).
[e] Reference 53.
[f] G. T. Ewan and A. J. Tavendale, Can. J. Phys. 42, 2286 (1964).

intensity ratio; we have no explanation for the disparity just mentioned. More recent results by Anderson *et al.* substantiate our results.[51]

E. Analysis of the hfs of Bi

None of the transitions observed in Bi exhibits a clearly resolvable hf splitting; both the $E2$ and $M1$ effects merely lead to more or less appreciable line broadenings. It is therefore important that the calibration (unsplit) line shapes used in the prediction of these broadenings, i.e., in the analysis of the experiment, be reliably known. We considered it essential to use exclusively calibration lines observed *simultaneously* with the Bi lines under investigation. Past experience in this laboratory has convinced us that it is virtually impossible to collect calibration events that are not beam-associated (e.g., γ rays from radioactive sources) under exactly the same conditions as muonic x rays.

K doublet. Here the calibration line was provided by the $K\alpha_1$ transition from a Pb^{206} target. The observed line was viewed simultaneously with the Bi target. Its observed line shape (Fig. 6) was corrected[54] for the isotope impurities (12%) of this Pb^{206} target on the basis of the I.S.'s in Table VI; this correction amounted merely to a broadening by 5%, i.e., 0.5 keV. The hfs of the Bi K lines was predicted with certain assumptions, folded with this line shape, and the prediction fitted to the experimentally observed lines by least squares.

TABLE VIII. Values of A_1 and A_2 obtained from the K doublet of Bi^{209}.

Line analyzed	$A_1(1s_{1/2})$ (keV)	$A_2(2p_{3/2})$ (keV)	Nucl.[a] mixing	Isomer shift (keV)	χ^2 14 deg of freedom
$K\alpha_2$	2.5±0.5	···	0	···	11.6±5.3
	2.5±0.5	···	Yes	0	10.6±5.3
	1.8±0.5	···	Yes	5	18.0±5.3
					χ^2 28 deg of freedom
$K\alpha_1$	2.5±0.5	−3.9±0.4	0	···	35.4±7.5
	2.5±0.5	−3.9±0.5	Yes	0	31.9±7.5
	2.5±0.5	−3.7±0.5	Yes	5	26.7±7.5
	1.8±0.5	−3.7±0.5	Yes	5	19.1±7.5

[a] See Sec. II C for the parameters used.

The $K\alpha_2$ line ($2p_{1/2} \rightarrow 1s_{1/2}$) depends directly only on the $M1$ hfs, i.e., on the constants $A_1(1s_{1/2})$ and $A_1(2p_{1/2})$ discussed in Sec. II B. Its line shape was predicted for three different hypotheses, viz., (a) no nuclear mixing (Sec. II C); (b) nuclear mixing with the parameters mentioned in Sec. II C, but neglecting isomer shifts; (c) as in (b), but assuming an isomer shift of 5 keV for the de-excitation of $\frac{15}{2}^+$ level of the Bi nucleus. In all three cases, *both* constants A_1 just mentioned are needed for the prediction. For simplicity, $A_1(1s_{1/2})$ was retained as a free parameter while the ratio $A_1(1s_{1/2})/A_1(2p_{1/2})$ was assumed known, and numerically equal to 2.0. This particular value of the ratio corresponds to a specific model, but we believe that it is far less model-dependent than the constants themselves. (See Table I.) This is supported by Le Bellac's results.[7]

The $2p_{3/2}$ level has both $E2$ and $M1$ hfs. Thus the $K\alpha_1(2p_{3/2} \rightarrow 1s_{1/2})$ transition involves the constants $A_1(1s_{1/2})$, $A_1(2p_{3/2})$, and $A_2(2p_{3/2})$. This line was analyzed similarly to the $K\alpha_2$, except that $A_2(2p_{3/2})$ was left as a free parameter, while $A_1(1s_{1/2})$ was taken for each hypothesis from the analysis of the $K\alpha_2$ line. The $A_1(1s_{1/2})/A_1(2_{3/2})$ ratio was again taken as fixed, but in this case as equal to 4.

[54] The data discussed here are those of Ehrlich *et al.* (Ref. 1). The values for $A_2(2p_{3/2})$ and $A_1(1s_{1/2})$ from the $K\alpha$ lines were obtained from the Pb^{206} line shape before correction for isotopic contamination.

Table VIII gives the values for $A_1(1s_{1/2})$ and $A_2(2p_{3/2})$ obtained from the best fits for the three hypotheses, as well as the χ^2's of these fits. The $K\alpha_2$ results do not enable one to make a conclusive choice between the three hypotheses, since all three give reasonable fits. It is perhaps worth noting that the apparent value of $A_1(1s_{1/2})$ is decreased by $\sim$0.1 keV for each keV of isomer shift. The $K\alpha_1$ results again allow no clear-cut choice, but favor hypothesis (c). Here the apparent value of A_2 is changed by 0.04 keV for each keV of isomer shift.

We investigated the sensitivity of the values of A_1 and A_2 to the region of fit and found only very slight variation in the best values; a 20% increase in window width about the $K\alpha_2$ line produced less than a 0.05-keV change in A_1. We also examined the sensitivity of the values of A_1 and A_2 to the shape of the Pb^{206} calibration lines. A 5% uncertainty in its linewidth produced a 0.15-keV change in A_2. The errors in A_1 and A_2 quoted in Table VIII allow for the uncertainties in the calibration width, the window width, as well as in the statistics. The error in A_2 also reflects slightly the uncertainty in $A_1(1s_{1/2})$. Thus the accuracy of $A_2(2p_{3/2})$ was not seriously affected by the uncertainties in $A_1(1s_{1/2})$. On the other hand, the $K\alpha_1$ peak was not used in the final determination of $A_1(1s_{1/2})$, since it was less sensitive to this parameter.

L lines. The $L\alpha_1$ and $L\beta_1$ lines were analyzed using the line shape of the Pb^{208*} capture γ ray (2.6145 MeV) that falls right between them in energy. The two-dimensional analysis features of our setup (see Sec. III B) were particularly useful in isolating this line; this is illustrated by Figs. 11(a) and 11(b).

The hfs of the $L\alpha_1$ transition depends on the constants A_1 and A_2 for the $2p_{3/2}$ and $3d_{5/2}$ levels. The fit to the observed lined shape was performed neglecting nuclear mixing, and leaving only $A_2(2p_{3/2})$ as a free parameter. The value for $A_1(2p_{3/2})=0.58$ keV was taken over from the K doublet analysis, while the hf constants of the $3d_{5/2}$ state were computed as indicated in Table I. These constants are very small compared to the experimental linewidths, and furthermore (because of the small penetration) independent of the nuclear charge and magnetization distributions. The values for $A_2(3d_{5/2})$ and $A_2(3d_{3/2})$ were obtained following Wheeler's[25] procedure and are also listed in Table I. The corresponding A_1's are essentially point dipole values. As can be seen, the $A_2(2p_{3/2})$ values obtained from the $L\alpha_1(-3.7\pm0.6$ keV) and $K\alpha_1$ lines are in good agreement. Similarly, the value of $A_1(2p_{1/2})=1.2\pm0.5$ keV obtained from the $L\beta_1$ line is consistent with that assumed in the analysis of the K lines, i.e., 50% of $A_1(1s_{1/2})$.

In Table IX, we compare our experimental values[55] for the hfs constants with those published by a group at Columbia.[9] For the purposes of this comparison, we quote our constants as determined *neglecting* the nuclear-mixing phenomena; the Columbia results were obtained in this approximation. We believe, however, that nuclear mixing does in fact occur, and consider the constants derived allowing for this mechanism (see Table VIII) somewhat preferable.

TABLE IX. Comparison of experimental hyperfine constants (assuming no nuclear mixing).

		This experiment (keV)	Bardin *et al.*[a] (keV)
$A_1(1s_{1/2})$	$K\alpha_2$	2.5±0.5	1.6
	$L\alpha_1$[b]	2.4±1.0	···
$A_2(2p_{3/2})$	$K\alpha_1$	−3.9±0.4	−3.8
	$L\beta_1$	−3.7±0.6	···[c]
$A_1(2p_{1/2})$	$L\alpha_1$	1.2±0.5	···[c]

[a] Reference 9.
[b] This value for $A_1(1s_{1/2})$ is inferred from the measured value of $A_1(2p_{1/2})$ rom the $L\alpha_1$ line and the assumed ratio of $A_1(1s_{1/2})/A_1(2p_{1/2})=2$.
[c] Not analyzed.

V. INTERPRETATION AND DISCUSSION OF RESULTS

A. Isotope Shifts

The central question at hand is a comparison between the optical and muonic data. Only our $K\alpha_1$ results are accurate enough to make this comparison in a meaningful way. Table X shows that there is in fact an excellent agreement. Our results confirm that the observed I.S.'s are only about half of what one predicts on the basis of the $A^{1/3}$ law. Not only is there agreement in the relative

TABLE X. Pb K muonic x-ray isotope shift.

		Observed[a] (keV)	Theory[b] (keV)
206–207	$K\alpha_1$	3.73±0.32	7.7
	$K\alpha_2$	4.05±0.86	7.3
206–208	$K\alpha_1$	9.39±0.30	15.3
	$K\alpha_2$	9.30±0.89	14.6

Normalized I.S. ratios $\delta E/\delta E_{\text{std}}$

Muonic $K\alpha_1$ data	Optical data[c]
$\frac{(206\text{–}207)_{\text{obs}}}{(206\text{–}207)_{\text{th}}}=0.48\pm0.04$	$\frac{C_{\text{obs}}}{C_{\text{th}}}\beta\text{——}=0.46\pm0.07$
$\frac{(206\text{–}208)_{\text{obs}}}{(206\text{–}208)_{\text{th}}}=0.61\pm0.02$	$\frac{C_{\text{obs}}}{C_{\text{th}}}\beta\text{——}=0.60\pm0.07$

Relative I.S. ratios

$\frac{(206\text{–}207)_{\text{obs}}}{(206\text{–}208)_{\text{obs}}}=0.397\pm0.036$	$\frac{(206\text{–}207)_{\text{obs}}}{(206\text{–}208)_{\text{obs}}}=0.38\pm0.01$

[a] Corrected for reduced mass effect.
[b] Assumed Fermi charge distribution $\rho(r)=\rho(0)/[1+\exp(r-c)/0.228t]$, with $R_u=1.194\times A^{1/3}$ F and $t=2.1$ F, where $R_u\cong c^2+1.19t^2$.
[c] From a review by Brix and Kopfermann (Ref. 3) based on optical measurement by Steudel (Ref. 2).

[55] Preliminary results of an hfs analysis of muonic Bi^{209} were presented by R. B. Sutton at the International Conference on Electromagnetic Sizes of Nuclei, 1967, at Carleton University, Ottawa. These results were in excellent agreement with our findings.

TABLE XI. Pb I.S.'s in terms of the nuclear charge parameters.

I.S.	Transition	$\Delta c/c \times 10^4$ [a]
Pb^{207}-Pb^{206}	$K\alpha_1$	8.3±0.7
	$K\alpha_2$	9.5±2.0
Pb^{208}-Pb^{206}	$K\alpha_1$	21 ±1
	$K\alpha_2$	22 ±2

[a] $\Delta c/c$ was calculated fixing $t=2.1$ F and $c=6.7$ F for Pb^{206}.

shifts, where the sensitivity to polarization of the nucleus by the muon is lessened, but also in the absolute (but normalized) shifts which should be more sensitive to these effects.

Our theoretical predictions for the muonic x rays are based on a specific (Fermi distribution) model for the charge distribution of the nucleus, and the question arises as to whether our conclusions are model-dependent or not. As Bodmer[56] has shown, the atomic I.S. δE referenced to a standard I.S. δE_{std}, (i.e., a shift evaluated for an equivalent uniform distribution with radius $R_u=r_0A^{1/3}$) is proportional to the fractional increase of the radius $\delta R_u/R_u$, viz.,

$$\beta\frac{C_{\text{obs}}}{C_{\text{th}}}=\frac{\delta E}{(\delta E)_{\text{std}}}=\frac{3A}{\delta N}\frac{\delta R_u}{R_u}. \tag{29}$$

Furthermore, Hill and Ford[57] have shown (by explicit numerical calculations for Pb) that the muonic $K\alpha$ energies vary linearly with nuclear range parameter (R_u) for small changes ($\sim 0.1\%$) in this parameter, and that for those charge distributions which yield the observed absolute transition energies, the sensitivity to these small changes in R_u is essentially model-independent.

Table XI lists the changes in the Fermi half-density radius c implied by the observed I.S.'s, assuming no change in skin thickness t.

The observed agreement between the optical and muonic data strongly suggests (1) that the theoretical interpretation of the optical results has been vindicated, and (2) that there is no evidence (at least in so far as the Pb isotopes 206, 207, and 208 are concerned) for appreciable nuclear polarization by the muon.

We are aware of some elastic electron scattering data[58] for Pb^{207} and Pb^{208}, but a comparison of results could not be interpreted in terms of a change in the radial charge-distribution parameter.

B. Inferred Quadrupole Moment of Bismuth

The currently quoted[59] value for the g.s. quadrupole moment of Bi^{209} is $Q=-0.34$ b. The values for Q originally quoted by the authors of optical[15] and atomic-beam[16] measurements are listed in Table XII (where each value has been corrected for the Sternheimer[60] effect); no errors are quoted in Refs. 15 and 16, presumably because of the theoretical uncertainties (see Kopfermann[22]) in calculating the relevant electric field gradients at the nucleus. These data have been re-interpreted by Korol'kov and Makhanek,[17] yielding 15% lower values. We do not feel qualified to decide which of the two interpretations is the correct one, but prefer to offer an alternative approach.

Let us consider how the data at hand can be interpreted.[61] Let us first treat Bi^{209} as consisting of a spherical Pb^{208} core and a single proton in an $h_{9/2}$ orbital. As we have shown in Fig. 2, such a model can at most produce an $E2$ hfs constant $A_2(2p_{3/2})=-3.8$ keV. But this maximum would correspond to a $Q\approx -1$ b, i.e., to an $E2$ moment almost *three times larger* than the one observed in ordinary atoms. On the other hand, if we fix Q at this latter value, then the single-particle model predicts $A_2\approx -2.8$ keV, i.e., about $\frac{2}{3}$ of what is observed (see Table XII) with muonic x rays. In other words, one cannot obtain a consistent picture of Bi^{209} within the framework of this simple model.

As a better description of Bi^{209}, we may try to attribute a slight deformation to the Pb^{208} core, while retaining the $h_{9/2}$ single proton (Rainwater[62] model). The deformation is here attributed to the attraction by the single proton. The contribution of a slight elliptical core deformation to A_2 is also shown in Fig. 2. It is evident that quite modest deformations (defined in Sec. II B) will make rather sizeable contributions to A_2. Thus in this model only a part Q_{sp} of the total moment Q is contributed by the lone proton. Figure 13 illustrates (among other things) this decomposition for *fixed* (viz., the observed) *values of* A_2. If both Q and A_2 were known exactly, one could read a unique Q_{sp} off this graph. This not being the case, one has to rely upon additional information to determine Q_{sp}.

We have obtained such information in two ways, using (1) the electron scattering value for $\langle r^2\rangle^{1/2}$, and (2) the muonic isotone shifts measured in this experiment.

TABLE XII. Quadrupole moment Q of Bi^{209} (barns).

Interpretation by	Authors of expt	Korol'kov and Makhanek[a]
Measurement		
Optical[b]	−0.40 (OG)[d]	−0.34 (OR)
Atomic beam[c]	−0.35 (ABG)	−0.30 (ABR)

[a] Reference 17.
[b] Reference 15.
[c] Reference 16.
[d] The abbreviations in parentheses following each value are used to identify these values of Q in Fig. 13.

[56] A. R. Bodmer, Nucl. Phys. **9**, 371 (1958).
[57] D. L. Hill and K. W. Ford, Phys. Rev. **94**, 1617 (1954).
[58] G. A. Peterson, J. F. Ziegler, and R. B. Clark, Phys. Letters **17**, 320 (1965).
[59] G. H. Fuller and V. W. Cohen, *Nuclear Data Sheets*, compiled by K. Way *et al.* (Printing and Publishing Office, National Academy of Sciences–National Research Council, 1965), Appendix 1.
[60] R. Sternheimer, Phys. Rev. **84**, 244 (1951).
[61] For a more complete discussion, see R. J. Powers and V. L. Telegdi, Z. Physik **202**, 214 (1967).
[62] J. Rainwater, Phys. Rev. **79**, 432 (1950).

Using the electron scattering value[30] of the mean-square radius of Bi^{209}($\langle r^2\rangle^{1/2}=5.51\pm0.06$ F), one obtains the shell-model length parameter α from the relation

$$\langle r^2\rangle=400/83\alpha^2. \tag{30}$$

From this and Eq. (15) we deduce

$$Q_{sp}=-0.298\pm0.006 \text{ b}. \tag{31}$$

This value is indicated in Fig. 13 by an arrow marked E.S. With this Q_{sp}, our experimental value of $A_2=-3.9$ keV implies (if we neglect the effects of nuclear mixing discussed in Sec. II C)

$$Q=-0.39\pm0.04 \text{ b}; \tag{32}$$

allowing for nuclear mixing, it corresponds to

$$Q=-0.37\pm0.05 \text{ b}. \tag{33}$$

The second method of attacking this problem is based on the following: Since the difference in $K\alpha$ energies of Pb^{208} and Bi^{209} is, to a good approximation, due to the Coulomb interaction of the extra proton with the muon in the $1s$ state—the effects of the Pb^{208} cores cancelling—one can determine, following Greiner and Scheck,[63] the length parameter α (and hence Q_{sp}) from the measured It.S. $\Delta K_{\alpha i}$ of either K_α transition ($i=1,2$). We computed the It.S. using relativistic muon wave functions for Pb^{208} described by a Fermi-type charge distribution, with $c=6.70$ F and $t=2.14$ F (these correspond to our observed x-ray energies). Even if the extra proton had no Coulomb interaction with the core, there would be a volume effect (analogous to an I.S.). We used the average I.S.'s from Pb to correct (by -4.6 keV for $\Delta K\alpha_1$ and -4.7 keV for $\Delta K\alpha_2$) for this effect. Another small but uncertain correction has to be made for possible differences in nuclear polarization by the muon; we applied the correction suggested by Scheck,[64] viz., -3.2 ± 1.1 keV. With these corrections, one predicts the connection between the isotone shifts and Q_{sp} indicated in Fig. 13 by the two slanted dashed lines. The two horizontal bands in this figure represent the observed isotone shifts (see the end of Sec. IV B) with their errors. The interaction of the slanted dashed lines with these bands yields the ranges of Q_{sp} values consistent with the observed isotone shifts. Numerically, these are

$$\begin{aligned} Q_{sp}&=-0.265\pm0.017 \text{ b} \quad (K\alpha_1)\\ &=-0.263\pm0.020 \text{ b} \quad (K\alpha_2). \end{aligned} \tag{34}$$

These values are in reasonable agreement with Eq. (31), as indicated by the arrow marked E.S. in the figure.

Finally, there might be a correction for the fact that we computed the It.S. for a *spherical* Pb^{208} core, while it is actually slightly deformed. We convinced ourselves by an explicit calculation that this correction is negligibly small; a core quadrupole moment of -0.1 b leads to a change in Q_{sp} of only 1%.

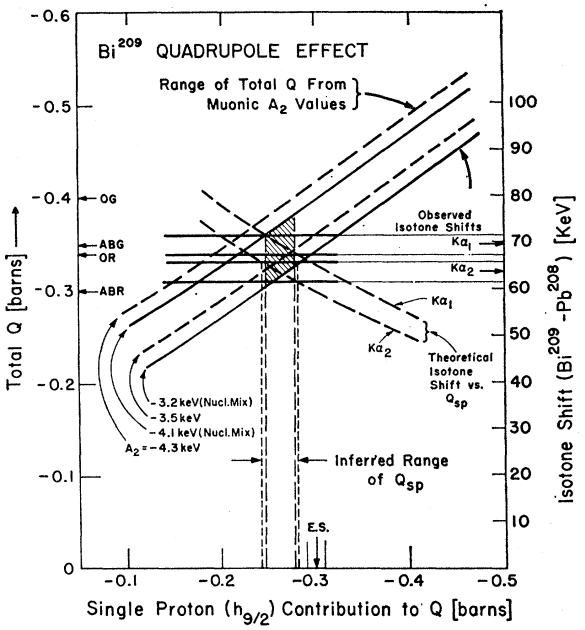

FIG. 13. Left-hand scale: The four curves with positive slope display the total Q of Bi, for a given value of the muonic A_2, as a function of its single proton part. The solid curves correspond to those values of A_2 assuming nuclear mixing; the dashed curves correspond to no nuclear mixing. Right-hand scale: The pairs of horizontal lines denote the observed isotone shift with error for the $K\alpha_1$ and $K\alpha_2$ transitions. The dashed curves with negative slope show the dependence of the isotone shift on Q_{sp}. The vertical dashed lines indicate the range of Q_{sp} consistent with the observed isotone shifts. The hatched area indicates the ranges of total Q and Q_{sp} consistent with both the A_2 values and the isotone shifts.

The hatched area in Fig. 13 corresponds to the range of values of Q_{sp} and Q that are consistent with both the observed It.S. and the observed hfs interaction constant A_2. Thus the "best" value for Q_{sp} is

$$Q_{sp}=-0.264\pm0\,013 \text{ b}, \tag{35}$$

which implies, for $A_2(2p_{3/2})=-3.9\pm0.4$ keV,

$$Q=-0.36\pm0.04 \text{ b}. \tag{36}$$

Nuclear mixing lowers the value of A_2 to -3.7 ± 0.5 keV;

$$Q=-0.35\pm0.05 \text{ b}. \tag{37}$$

In conclusion, we believe that the muonic data, both the observed value of $A_2(2p_{3/2})$ and the It.S., suggest that about 30% of the quadrupole moment of Bi^{209} is due to an induced core deformation, this deformation being of the order of $\sim1\%$. Our conclusion is corroborated by the earlier work of True,[65] who analyzed experimental electromagnetic transition rates in Bi^{209} in terms of the Rainwater[62] model, and found a core contribution of about 50%.

[63] W. Greiner and F. Scheck, Nucl. Phys. **41**, 424 (1963).
[64] F. Scheck, Z. Physik **172**, 239 (1963).
[65] W. W. True, Phys. Rev. **101**, 1342 (1956).

Although no single experiment can be said to give convincing proof for the existence of a distorted core, it is indeed encouraging that three completely independent methods give consistent results.

There were some simplifications in our discussion. Although we do not believe that these could vitiate our main argument, we believe it best to list those of which we are aware: (1) uncertainties in the radial shape of the lone proton distribution, especially neglect of configuration mixing and relativistic effects; (2) uncertainties in the polarization effects[63] in the computation of the isotone shift.

C. Magnetic Hyperfine Effect

In our opinion, the most reliable value of $A_1(1s_{1/2})$ is obtained by allowing for nuclear mixing with a finite isomer shift (see Sec. II C, in particular Table VIII). Unfortunately, the precise value of $A_1(1s_{1/2})$ depends on the magnitude of the isomer shifts, viz., it changes by 0.13 keV for each keV of this shift, and the latter is neither known experimentally nor predicted theoretically at present. Assuming that the isomer shifts in question do not exceed the (known) isotope shifts in this region of the periodic table, we conclude that 5 keV represents an upper limit for them. For the purposes of quoting the "best" value for $A_1(1s_{1/2})$, we shall therefore tentatively *assume an isomer shift of 3 keV*. This hypothesis yields

$$A_1(1s_{1/2}) = 2.1 \pm 0.5 \text{ keV},$$

to be compared with the predicted values

$$A_1(1s_{1/2}) = 3.1 \text{ keV (point dipole)}$$
$$= 2.0 \text{ keV (extended dipole)}.$$

Although the evidence is admittedly not too strong, our results favor a distributed dipole. In view of the present limited experimental accuracy in A_1, it would be premature to discuss the influence of nuclear structure[6] on this quantity, in particular to consider configuration mixing[7] which is a 20% effect.

Using a Ge(Li) detector of better resolution than ours (8 keV for the 6130-keV O^{16*} line as compared to our 10.5 keV), Bardin *et al.*[9] have also determined $A_1(1s_{1/2})$ for Bi. They used for line-shape calibration the O^{16*} γ just mentioned, as recorded intermittently throughout their experiment, and concluded (neglecting nuclear mixing) that configuration mixing gives a slightly ($\lesssim 8\%$) better χ^2 than the pure shell model. In light of Columbia's stated 12% uncertainty in the width of their calibration line ($8 \rightarrow 9$ keV), we believe that the above conclusion holds for the Columbia experiment as well. However, considering the A_1 values (see Table IX) of the two experiments jointly enables us to rule out the point-dipole model.

ACKNOWLEDGMENTS

I would like to thank Professor V. L. Telegdi for suggesting this problem and for his generous encouragement and participation in the preparation, performance, and interpretation of this experiment. I thank my collaborators Richard Ehrlich, David Fryberger, Douglas Jensen, Charles Nissim-Sabat, and Bruce Sherwood for contributing much effort, time, and thought toward the completion of this experiment. I would also like to thank Richard Ehrlich for many discussions contributing to my understanding of the results. I am indebted to H. Mann and his group at Argonne National Laboratory for supplying and maintaining the Ge(Li) detector used in this experiment, and to Tom Nunamaker of this Institute for generously providing his design skills. I appreciate an informative communication with Dr. M. Le Bellac. I am grateful to Professor H. Anderson and R. J. McKee for allowing me to use their computer program to calculate Dirac muon wave functions. I thank Ron Swanson and Karl Sebesta for technical assistance. Finally, I thank Mrs. Elizabeth Bitoy for her unending patience in typing the numerous drafts for this paper.